LAPORAN PENELITIAN

CHITOSAN-ALGINATE POLYELECTROLYTE COMPLEXES FOR ENCAPSULATION OF LOW MOLECULAR WEIGHT FISH BIOACTIVE PEPTIDES

YONI ATMA, S.TP., M.Si., Ph.D
NIDN: 0317038602

PROGRAM STUDI ILMU DAN TEKNOLOGI PANGAN

UNIVERSITAS TRILOGI

JAKARTA

2025

ABSTRACT

Our study focuses on improving the encapsulation of bioactive peptides (BAPs) by exploring electrostatically mediated macromolecular aggregates of two polysaccharides. Current systems often suffer from premature cargo release due to factors such as the action of digestive enzymes and pH swings. To address this, we have developed Polyelectrolyte Complexes (PECs) from non-digestible chitosan (CS) and sodium alginate (ALG) via a one-step mixing process. The resulting PECs were characterized via dynamic light scattering (DLS), mixed-mode phase analysis light scattering (M3-PALS), and small-angle X-ray scattering (SAXS). Subsequently, we used two PECs, one with an excess of CS and another with an excess of ALG, to encapsulate low molecular weight (M_w) fish BAPs, quantifying their encapsulation efficiency (EE) and release patterns at both gastric and intestinal pH levels via HPLC-UV/Vis analysis. The morphology of the loaded PECs was also investigated via transmission electron microscopy (TEM). We found that the PEC hydrodynamic radius (R_h) depends on the charge ratio (CR) (n-/n+). At low n-/n+ ratios (0.1 to 0.6), R_h reduced from approximately 800 to 300 ± 50 nm, indicating more compact structures. The □-potential also changed with n-/n+. The role of ALG M_w was explored, supported by SAXS results and provided insights into the structural diversity achievable using this simple complexation method. Importantly, our PECs demonstrated EE values of 80 to 85% and controlled release of less than 10% at pH 3.0 and less than 20% at pH 6.8, after 3 h. TEM analysis showed that the loaded PECs ranged in size from less than 50 nm to over 10 µm. This research highlights the potential of such PECs as effective carriers for low M_w fish BAPs, offering controlled release and enhanced protection against premature degradation. It represents a significant advancement in BAP delivery and encapsulation technology.

Keywords: alginate, chitosan, digestion, fish peptide, polyelectrolytes

I. INTRODUCTION

Bioactive peptides (BAPs), typically composed of 2-20 amino acids, exhibit bioactivities relating disease prevention, promoting human health, and supporting physiological functions (Guo et al., 2023; Nongonierma & FitzGerald, 2015; Patil et al., 2022). The majority of BAPs are derived from enzymatically hydrolysed proteins (Han et al., 2021; Lorenzo et al., 2018) sourced from natural origins such as dairy products (Estévez et al., 2020; Nongonierma et al., 2019; Yan et al., 2019), meat (Cao et al., 2020; Xing et al., 2019), fish (Abdelhedi et al., 2017; Neves et al., 2017), eggs (Marcet et al., 2022; Moreno-Fernández et al., 2020), plant proteins (Han et al., 2019; Kumar et al., 2022; Piovesana et al., 2018; Yuan et al., 2022), algae (Cermeño et al., 2020; Harnedy et al., 2017), insects (Ma et al., 2023; Sousa et al., 2020), and mushrooms (Zhou et al., 2020). Fish and by-products from fish processing stand out as potent sources of BAPs, showcasing bioactivities encompassing antioxidant, antihypertensive, antimicrobial, and anti-inflammatory properties (Gao et al., 2021; Halim et al., 2016; Le Gouic et al., 2019; Nirmal et al., 2022; Zamora-Sillero et al., 2018). Notably, antihypertensive BAPs from marine sources surpass other bioactivities, with some supplements containing these peptides commercially available (Fuentea et al., 2020; Hayes & Tiwari, 2015). The burgeoning interest in fish BAPs underscores their potential to enhance health and prevent diseases, marking a significant stride in the development of functional foods and nutraceuticals.

A notable antihypertensive Bioactive Peptide (BAP) with pronounced bioactivity is the pentapeptide LKPNM (leucine-lysine-proline-glutamine-methionine), derived from the muscle of bonito fish through thermolysin hydrolysis. This specific BAP, presented in the form of a food supplement, has undergone patenting, and literature has detailed the sequence of BAPs within this patented product (Curtis et al., 2002; Fujita & Yoshikawa, 1999). The LKPNM does not exhibit a bitter taste (Yokoyama et al., 1992). However, it is noteworthy that, to date, there is a dearth of published research on the encapsulation of this particular BAP. It is widely acknowledged that encapsulation of BAPs for applications in food, food supplements, and nutraceuticals is imperative to shield them from undesired hydrolysis and degradation, preserving their intact sequences and bioactivities (Basirico et al., 2015; Fernández-Musoles et al., 2013; Lacroix et al., 2017). Moreover, given the susceptibility of peptides to gastrointestinal challenges in their unencapsulated state, addressing this vulnerability becomes crucial. Prior investigations predominantly centered on the encapsulation of insulin or proteins considerably larger than BAPs (Aguilar-Toala et al., 2022; Feng et al., 2019; Mohan et al., 2016; Mohan et

al., 2015; Y. W. Zhang et al., 2021), and often exceeding their size by at least tenfold. While some attempts have been made to encapsulate short BAPs, ranging from di- to decapeptides, the prevalent use of chitosan (CS) as an encapsulating material has been noted (Bicak et al., 2021; Chen et al., 2017; Danish et al., 2017), and noteworthy, when combined with alginate (ALG), the composite material serves as a protective carrier, mitigating premature release of BAPs (Huang et al., 2017; Xiao et al., 2017).

Chitosan (CS) is an amino polysaccharide obtained from chitin which is among the most abundant biopolymers in nature (along with cellulose). CS is obtained at commercial scale by partial thermoalkaline N-deacetylation of chitin (Alonso & Goycoolea, 2008). Chitin is mostly found in the exoskeleton of crustaceans like crab and shrimp or their waste, and also found in molluscs, insects, and fungi. Production CS from these sources is inexpensive (George & Abraham, 2006). CS structure is described as a linear polysaccharide consisting of glucosamine (deacetylated units, D) and N-acetyl-glucosamine (acetylated units, A) units via β-(1→4) linkages (Potaś et al., 2020) (Figure 2a). The molar fraction of A residues to the total (A+D), defines the degree of acetylation expressed as fraction of acetylation (F_A). The distribution of A residues in CS, known as the pattern of acetylation, in chemically deacetylated CS is known to be random, but using enzymatic technology, it is possible to produced blockwise patterned CS (Wattjes et al., 2020). The other parameter that dictates CS's properties and applications is the molecular weight distribution. This is expressed by the weight average molecular weight (M_w), the number average molecular weight (M_n) and the polydispersity ($M_w/M_n = Đ$). The positive charge of CS is due to the amino groups that become protonated at pH below its pKo (~6.1) and drive its solubilisation in mild aqueous solutions (Maciel et al., 2017). Otherwise, CS is insoluble in both water and organic solvents. Generally, commercial CS show a F_A of 0.05 to 0.30 and molecular weight between 10 and 500 kDa (Luo & Wang, 2014).

CS has been widely used in food and pharmaceutical industries. CS has superior properties as an encapsulation agent including for oral or gastrointestinal delivery. It is because they are biodegradable, biocompatible, mucoadhesive, permeation enhancer, and easy to modify. CS increases the bioaccessibility and bioavailability of encapsulated protein and peptides during gastrointestinal delivery because the mucoadhesive ability makes they can penetrate into intestinal mucus layer pores. CS enables to open tight junction and enhance absorption into paracellular route of intestinal epithelium (Sonaje et al., 2012). Due to its positive charge at mildly acidic conditions, and many natural polymers exhibit negative

(polyanionic) charge in this pH range, CS forms complex with polyanions by means of electrostatic interactions. For instance, alginate (ALG) has been complexed with CS and proven improve the chitosan stability at various pH (Potaś et al., 2020).

ALG is an anionic polysaccharide that is commercially extracted from brown seaweeds. The polyanionic charge of ALG is given by their carboxyl groups. ALG is unbranched biopolymers consisting of (1→ 4) linked α-guluronic acid (G) block and β-mannuronic acid (M) block (Goycoolea et al., 2009). The sequences of polymer are homosequences (M blocks and G blocks) interspersed with heterosequences (G-M blocks) (Figure 2a) with molecular weight between 60 and 700 kDa. ALG is water soluble capable of forming gels whether by decreasing pH or by addition of specific divalent cations such as Ca^{2+} to form Ca-ALG (Pravinata & Murray, 2019). Their mannuronic and guluronic (M/G) ratio and molecular weight affect its physical properties (Cazorla-Luna et al., 2021). ALG has been used extensively in food industries and it is approved as GRAS (Generally Recognized as Safe) food hydrocolloid by FDA. ALG has been developed as microgel particles via simple one step process for protein lactoferrin encapsulation (Pravinata et al., 2016). Currently, ALG is the one biopolymer that mostly developed for biomaterial applications.

In terms of encapsulation agent for gastrointestinal delivery, ALG offers many advantages. These include its mucoadhesive character (George & Abraham, 2006; Gombotz & Wee, 1998), low toxicity, biocompatible, unhydrolyzed by most enzymes in gastrointestinal tract. Furthermore, the polyanionic charge of ALG supports its ability to entrap cationic BAPs. In addition, the anionic charge of ALG confers it the ability to associate electrostatically with cationic biopolymers such as chitosan and form PECs. ALG, CS, and peptide-based PECs are promising candidate systems for gastrointestinal delivery. Polycationic and polyanionic interaction chitosan and ALG enable them to create multiple layers of complex delivery. Some studies have proven that crosslinking ALG with CS reduces the porosity of ALG hydrogels, thus preventing peptide leaching, diffusion, and reducing peptide release in gastric juice (George & Abraham, 2006; Luo & Wang, 2014; Potaś et al., 2020). Concerning short-chain BAPs encapsulation, CS has been studied to encapsulate in sole and composite form with ALG. CS NPs used to encapsulate IPP, LKP, ECG, YKT with ionic/coacervation method (Bicak et al., 2021; Danish et al., 2017; Trapani et al., 2010). CS/ALG have studied to encapsulate KPV by double emulsions solvent evaporation method (Xiao et al., 2017) and to encapsulate VLPVP by membrane emulsification combined ionic gelation (Huang et al., 2017).

The encapsulation of BAPs through the CS and ALG via ionic interaction results in the formation of a Polyelectrolyte Complex (PEC). The utilization of PECs for BAPs delivery offers numerous advantages, such as being a straightforward, versatile, and cost-effective technique, particularly in terms of its suitability for industrial applications. Furthermore, PECs can be customized to regulate release patterns and facilitate targeted delivery. This study focuses on presenting the biophysical properties of CS-ALG PECs, the interaction, both unloaded and loaded, encapsulation efficiency, and investigates their release profiles under gastric and intestinal pH levels.

II. MATERIAL AND METHODS

1.2 Materials

Chitosan M_w 110 kDa, degree of acetylation (DA)=10% (HMC^+), Alginate M_w 21 kDa mannuronic (M) to guluronic (G) acid (M/G) ratio 1.42, Alginate M_w 8 kDa M/G ratio 5.1 (Danisco), Fish (bonito) protein extract PeptACE® (Natural Factors, USA), synthetic peptides; LKPNM and LKP (GenScript, ≥95% HPLC), Milli-Q water, Acetonitrile (ACN) (Sigma-Aldrich, HPLC grade), and Trifluoroacetic acid (TFA) (Alfa Aesar, HPLC grade 99.5%), sodium chloride (NaCl), and hydrogen chloride (HCl), milli-Q water, and distilled water.

2.2 Low molecular weight fish BAPs Preparation

Isolation of short fish BAPs carried out by weighing 2 g fish (bonito) protein extract PeptACE®, then dissolved in 100 mL distilled water (0.02%, m/v) and followed with stirring at room temperature for 60 minutes. After that, the dissolved solution centrifuged at 5.000 x g (Hettich, Ritona 380 R, 457 x 600 x 418 mm) for 30 minutes at 4 ºC. Subsequently, the supernatant collected and fractionated by filtering it using Ultracel® filter molecular weight cut off (MWCO) 3 kDa ultrafiltration disc (Amicon® Bioseparations). Next, the filtered fractionation solution (≤3 kDa) stored at 4 ºC before further identification and purification. Purification and analysis of fractionated (≤3 kDa) solution carried out by using high-performance liquid chromatography (HPLC) (Shimadzu, Japan) with reverse-phase (RP) technique. The fractionated solution diluted ten times with Milli-Q water and filtered through a 0.22 µm hydrophilic PVDF syringe filter. Afterwards, they were loaded into an autosampler tube (vial 1 mL). RP-HPLC was performed based on Curtis et al. (2002), Jiang et al. (2017), and Liu et al. (2020) with some modifications, using C-18 column stationary phase (Gemini®, 4.6x250 mm, 5 µm, 110 Å) flow rate 1 mL/min, mobile phase A was Milli-Q water, and B was Acetonitrile (ACN) containing 0.05% Trifluoroacetic acid (TFA). The gradients mobile phase for ACN was 5% (0-6 minutes), 15% (6-10 minutes), 25% (10-15 minutes), and 35% (15-21 minutes). The injection volume was 20 µL. The eluent was measured at wavelength (λ) 219 nm. The samples were compared with retention time of standard solutions: LKPNM and LKP (GenScript, ≥95% HPLC). The remaining of fractionated solution was freeze-dried and keep on the fridge until next steps.

2.3 Preparation of The Stock Solution

A 250 mg CS dissolved in 50 mL 85 mM NaCl (Goycoolea et al., 2009) to get 10 mg/mL CS solution. Then HCl added to obtained 25% stoichiometric excess of HCl. ALG also

dissolved into 25 mL 85 mM NaCl to get similar concentration with CS. On both solutions, 0.02% v/v sodium azide added as preservative. Then subsequently stirred 250 rpm, overnight at room temperature. After totally dissolved, the 10 mg/mL CS and ALG filtered using hydrophilic polyethersulfone (PES) sterile membrane (Millex®, Millipore, Ireland) pore size 0.22 µm, diameter 33 mm, then their density measured with density meter (Anton Paar GmbH, Austria) at 25 °C. The density of CS and ALG at series concentration (0, 1.0, 2.0, 3.0, 4.0, 5.0 mg/mL) without filtering also measured with density meter to get standard curve, then the concentration of CS and ALG after filtration precisely calculated. Concentration CS and ALG after filtration also setting up by adding certain amount of filtered (0.22 µm membrane filter) 85 mM NaCl solution. Figure 1 illustrates stock solution preparation and their density measurements.

2.4 Stoichiometric Charge Ratio (CR) Calculation

Preparation of PECs was by setting their CR adopted from Magalhaes et al. (2016) and Maciel et al. (2017) methods with some additions particularly for ALG charges. Charges of CS and ALG defined as equivalent molar mass per charge (**Eq**), according to formula 1 and formula 2 below, where are,

$$\text{CS,} \quad Eq_{CS} = \frac{M_{CS}}{1-(\frac{DA}{100})} \tag{1}$$

$$\text{ALG,} \quad Eq_{ALG} = \frac{M_{ALG}}{\text{Number charge per residue}} \tag{2}$$

Whilst the average molar mass (M_{CS}) of CS depends on degree of acetylation (DA), with the formula:

$$M_{CS} = 162.16 \text{ x } [1-\left(\frac{DA}{100}\right)] + 204.09 \text{ x } \left(\frac{DA}{100}\right) \tag{3}$$

In turn, the molar mass of ALG (M_{Alg}) = $\sum Ar$ of $[C_6H_8O_6]$. After that, number **Eq** molar mass per mol/concentration calculated by using concentration of CS or ALG (mg/mL) as numerator and **Eq** equivalent molar mass per charge as denominator**.** Furthermore, stoichiometric charge ratio ALG/CS $[n^-/n^+]$ determination started from CR 1, while the concentration, Eq charges, and total volume are parameters used for calculation. The formula total volume CS and ALG which added to tailoring their CR or $[n^-/n^+]$ ratio outlined below:

$$\text{ALG volume} = 1\text{ALG}_{\text{Vol}} = \frac{\left(\frac{\text{EqCS}}{\text{EqALG}}\right) \text{x Vol Total}}{1+\left(\frac{\text{EqCS}}{\text{EqALG}}\right)} \quad (4)$$

Then volume for CS at CR 1,

$$1\text{CS}_{\text{Vol}} = \text{Tot}_{\text{Vol}} - 1\text{ALG}_{\text{vol}} \quad (5)$$

Afterward, volume CS at CR 1 (1CS_{Vol}) and ALG at charge ratio 1 (1ALG_{Vol}) used to calculate volume ALG and CS for CR's lesser than 1 (< 1) or higher than 1 (> 1), for example at charge ratio 0.1,

$$\text{Therefore, } 0.1\text{ALG}_{\text{vol}} = \frac{1\text{ALG Vol x } 0.1}{(1\text{ALG Vol x } 0.1+1\text{CS Vol})\text{x Tot Vol}} \quad (6)$$

then volume CS at CR 0.1, $0.1\text{CS}_{\text{vol}} = \text{Tot}_{\text{Vol}} - 0.1\text{ALG}_{\text{vol}}$ (7)

Or at charge ratio 5,

$$\text{So, } 5\text{ALG}_{\text{vo l}} = \frac{1\text{ALG Vol x } 5}{(1\text{ALG Vol x } 5 + 1\text{CS Vol})\text{x Tot Vol}} \quad (8)$$

And, the volume CS at CR 5, $5\text{CS}_{\text{vol}} = \text{Tot}_{\text{Vol}} - 5\text{ALG}_{\text{vol}}$ (9)

2.5 Polyelectrolyte Complex (PEC) and Fish BAPs loaded into PECs

The unloaded PEC preparation carried out by one step mixing technique (Goycoolea et al., 2009) whereas volumes of ALG solution added into CS solution according to the CR calculation as illustrated above with total volume 2 mL. Then the suspension containing CS-ALG was vortexed and incubated at room temperature for 3 h. After that, the PECs sonicated for 5 minutes (5 seconds pulsed ON, 3 seconds pulsed OFF) at 4 ^{o}C amplitude (AMP) 35%, 20 kHz using ultrasound Sonics® VCX 750 (Sonics & Materials, Inc, Newtown, CT, USA) coupled with tapered microtip probe. While for the loaded PECs, the fish BAPs dissolved in filtered milli-Q water 1.0 mg/mL, then added as much as 200 µL into CS solution. After mixing, subsequently the ALG solution added into suspension containing CS-BAPs, vortexed, and followed by incubation at room temperature for 3 h. The sonication stage, carried with the same condition as what the unloaded PECs treated. For the selected PECs, both loaded and unloaded formulation were transferred into new Eppendorf containing small amount glycerol (dispense 5 drops using a 1 mL syringe needle) in the bottom part, then centrifuged at 20,000 x g for 25 minutes. The supernatant discarded, and the pellet resuspended with 400 µL 85 mM NaCl.

2.6 Encapsulation Efficiency (EE)

Loaded PECs solution after sonication was then centrifuged at 20,000 x g for 25 minutes. The supernatant collected and put into HPLC vial, then the BAPs quantified with HPLC-UV/Vis (Agilent, Germany). The HPLC performed as method explained above (section 2.2). Before running samples, the standard BAPs ran first with concentration 0 until 2.5 mg/mL first, since in these concentrations range the peaks had detected and urea under the curve had quantified. Finally, the EE defined as concentration of BAPs quantified in the supernatant divided by initial concentration multiply by 100% (Bicak et al., 2021; Danish et al., 2017).

$$\text{EE (\%)} = \frac{\text{Total amount fish BAPs loaded - free amount of BAPs in supernatant}}{\text{Total amount fish BAPs loaded}} \text{ x } 100\% \qquad (10)$$

2.7 Release study

In vitro release study conducted at pH 3.0 and pH 6.8. This analysis adopted from (Goycoolea et al., 2009) with slight modification. The pellet after centrifugation resuspended with 3 mL 0.1 M HCl pH 3 and 0.1 M NaOH pH 6.8 respectively followed with incubation for 3 h at 37 ºC. After that, centrifuged at 20,000 x g for 25 minutes, then supernatant taken around 1 mL and free of fish BAPs in the supernatant quantified with HPLC-UV/Vis. Total release of BAPs determined by concentration of BAPs in the supernatant divided by initial BAPs that remaining on the PECs and multiply by 100%.

$$\text{Release (\%)} = \frac{\text{amount of fish BAPs release to the simulated medium}}{\text{Initial amount of fish BAPs on the complex before simulation}} \text{ x } 100\% \qquad (11)$$

2.8 Biophysical characterization

The particle size and polydispersity index analysed based on dynamic light scattering (DLS). Sample suspensions pipetted around 1 mL and placed into polymethyl methacrylate (PMMA) Cuvette UV Transparent, Semi-Micro Filling, Path 10mm (VWR International, UK) then were measured in the Zetasizer Ultra (Malvern Panalytical). The measurement performed by setting the cuvette mode on ZEN0040 and refractive index of dispersant 1.33 (water). Samples were equilibrated for 120 s at 25 ◦C and analysed using backscattered light at a detection angle of 173◦. The particles sizes were defined as hydrodynamic radius (R_h). The software employs the Stokes-Einstein equation to derive R_h from the diffusion coefficient (D), presuming the particles are spherical:

$$R_h = \frac{K_B T}{3 \pi \eta D} \qquad (12)$$

Where, K_B is Boltzmann's constant, T is absolute temperature, η is viscosity, and D is diffusion coefficient (O'Connell et al., 2023; Okeudo-Cogan et al., 2023).

The □-potential was determined from the electrophoretic mobility measured by mixed-mode phase analysis light scattering (M3-PALS). Samples were diluted into a buffer (100 µL sample in 5 mL 10 mM NaCl) and vortexed. Then 0.8 mL samples loaded into folded capillary zeta cell DTS1070, and subsequently measured using Zetasizer Ultra (Malvern Panalytical) equipped with a 4 mW He/Ne laser beam (λ = 633 nm) at 25 ◦C. The □-potential determined by Smoluchowski approximation:

$$\zeta = \frac{4\pi\,\eta\,\mu}{\varepsilon} \quad \text{in which, } \mu = \frac{V}{E} \qquad (13)$$

Where ζ is zetapotential, η is viscosity buffer, µ is electrophoretic mobility, ε is the electric constant of the solvent, ν is velocity, and E is electrical field (Doroszkowski, 1999; S. Zhang et al., 2021).

2.9 Small Angle X-ray Scattering (SAXS)

Small angle X-ray scattering (SAXS) conducted to confirm complex formation between CS and ALG. The analysis has been done on unloaded PECs. SAXS measurements were performed utilizing the SAXSpace small-angle X-ray camera provided by Anton Paar (Graz, Austria). Shortly, we use an X-ray beam that is collimated into a line focus, having a length of 20 mm and a width of 0.5 mm. The distance of sample to detector was around 317 nm, but the meticulous extent measurement was achieved through the utilization of silver behenate powder. Each sample was loaded into Quartz 1.5 mm capillary tube and exposed for 3600 s. The SAXS machine was fitted with an X-ray generator using a sealed-tube copper (Cu) anode, operating at 40 kilovolts (kV) and 50 milliamperes (mA), generating X-rays with a wavelength (λ) of 0.154 nm. The instrument system was additionally run in high-intensity mode, offering a minimum accessible scattering vector value, q_{min}, of 0.12 nm -1) (where $q = 4\pi/\lambda \sin(\theta)$, and 2θ represents the scattering angle). Entire unloaded complex explorations with SAXS were executed at a temperature of 25 ºC (Apostolidis et al., 2023).

2.10 Density and Viscosity

Density (ρ) assessments were conducted on a set of CS and ALG solutions with predetermined concentrations, established through weighing of them and made with serial concentrations. The acquired data were employed to create standard curve and the used to

validate the concentration of filtered CS and ALG stock solutions by means of additional density measurements. The measurements were undertaken using a DMA 4500 M density meter (Anton Paar GmbH, Austria), on CS and ALG solutions of concentration ranging from 0.001 to 0.005 g/mL wt %, at 25 ◦C (O'Connell et al., 2023). Measurements were carried out in three replications. Pure water and solvent (85 mM NaCl) initially measured to calibrate the instrument and to further ensure that the density remains unchanged. All solutions were loaded into the instrument uniformly, each comprising 1 mL dispensed using a 1 mL syringe, ensuring the absence of any bubbles during the measurement.

Viscosity (η) analysis of the supernatant from CS-ALG complexes was conducted to determine the remaining viscosity post-complexation (Menchicchi et al., 2014). Utilizing the microVISC™ by RheoSense, a 300 µL of the supernatant was loaded into the device, which is equipped with a chip featuring a rectangular slit for both inflow and outflow. The chip, enhanced with a sensory array, measures the solution's flow as it is propelled by a plugger, with viscosity recorded in millipascal-seconds (mPa s).

2.11 Electron Microscopy (EM)

Transmission electron microscopy (TEM) performed to observe the morphology (shape), size, and aggregation of the PECs. TEM imaging was undertaken on loaded PEC with excess CS since this system has smaller size, proper stability, and higher EE result. The sample solution mixed with Pasteur pipette and dropped twice into copper TEM grid which placed on filter paper, then allowed to dry and covered with clean petri dish. Then TEM grid containing sample placed carefully into TEM specimen holder by using a clean tweezer and the grid clamped. TEM analysis carried out using a FEI Titan3 Themis G2 S/TEM operated at 300 kV with energy spread approx. 0.25 eV and Gatan OneView 4K CMOS digital camera. TEM imaging performed with several magnifications (Nahi et al., 2022).

2.12 Statistical Analysis

The data outcomes were presented in the form of mean values accompanied by standard deviations. SPSS Statistics 29.0 (IBM, Chicago, IL) was employed for the data analysis. The efficacy of the treatment was assessed through a one-way analysis of variance (ANOVA), followed by the application of Tukey's test. Statistical significance was established at a threshold of $p < 0.05$.

III. RESULTS AND DISCUSSION

3.1 Fish Bioactive Peptides Fractionation and Identification

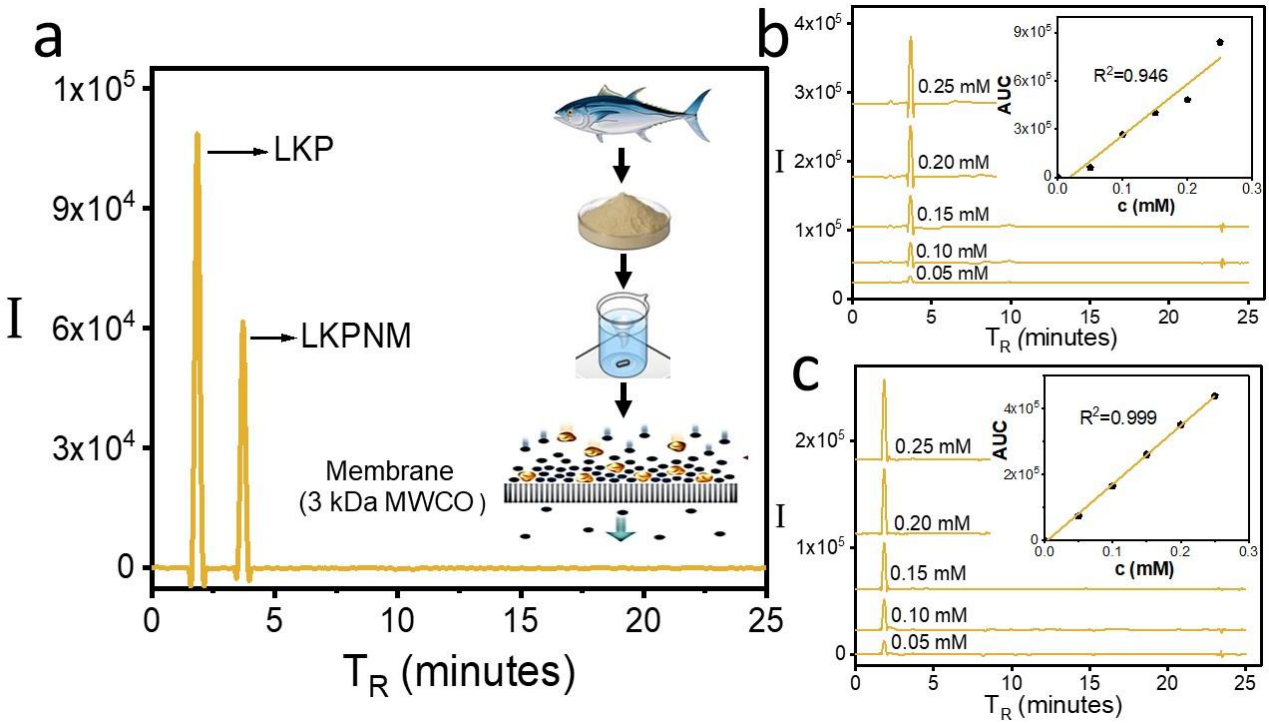

Figure 1 The RP-HPLC chromatogram of ≤ 3kDa fish BAPs and the fractionation schematic process (a). The standard curve for LKPNM (b) and LKP (c), ranging from concentration (c) 0.05 mM to 0.25 mM, reveals increased urea under the curve (AUC) and intensity with rising concentrations.

The peptides derived from fish were separated using ultrafiltration (UF) with a membrane disc of a molecular weight cutoff (MWCO) of 3 kDa to obtain a fraction solution containing BAPs with molecular weights (M_w) of ≤3 kDa. Identification of these peptides was conducted through Reverse Phase High Performance Liquid Chromatography (RP-HPLC) utilizing a C-18 stationary phase. Prior to sample injection, the column underwent washing and equilibration with the mobile phase, consisting of Milli-Q water and acetonitrile (ACN). The resulting HPLC chromatogram distinctly revealed two predominant peptides in the UF solution, characterized by high-intensity and sharp peaks. Specifically, elevated intensity was observed during retention times spanning 105 to 117 seconds and 218 to 225 seconds. Subsequently, two synthetic peptides; LKP and LKPNM (purity >95%) were introduced into the HPLC system under analogous conditions (identical mobile phase, flow rate, and stationary

phase). The chromatogram displayed analogous intensity at corresponding retention times. These synthetic peptides served as standards, and it was observed that increasing their concentrations (0.05-0.25 mM) resulted in a proportional augmentation of the area under the curve and intensity in the chromatogram. Notably, owing to its lower molecular weight (M_w) compared to LKPNM, LKP eluted slightly earlier, potentially due to higher solubility in the hydrophilic mobile phase and reduced interaction with the hydrophobic stationary phase. Consequently, our inference is that two primary short peptides are present in the derivatives of bonito fish. This outcome corroborates the composition of bioactive peptides (BAPs) in PeptACE®, specifically the presence of LKPNM, as elucidated in preceding studies (Curtis et al., 2002; Fuentea et al., 2020; Fujita & Yoshikawa, 1999). Additionally, the existence of LKP may stem from the hydrolysis of LKPNM, as indicated in a prior publication (Fujita et al., 2000; Fujita & Yoshikawa, 1999). The hydrolysis of LKPNM yielded two peptides: LKP and NM. Notably, LKP exhibited an eight-fold higher antihypertensive activity than the original pentapeptide (LKPNM), with an IC50 of 0.32 μM, while NM did not manifest any bioactivities. It is pertinent to note that no other synthetic short peptide was employed as a standard during this analysis. Fortuitously, the observation of these two dominant short BAPs was made. The chromatograms illustrating the BAPs in the PeptACE® product and the standards of synthetic LKPNM and LKP are presented in Figure 1.

While identifying the short fish peptide, no additional BAPs were observed, despite assertions in their patent claiming the presence of six short fish peptides (Guan et al., 2001). A study conducted by Curtis et al. (2002) reported that the BAPs in the PeptACE® product exhibit a high degree of purification, demonstrating 95% similarity with synthetic LKPNM through LC-MS analysis. Notably, PeptACE® comprises 85% peptides derived from dried Bonito fish, with an IC_{50} of 50.2 μg/ml (2.40 μM) for LKPNM. It is pertinent to mention that LKPNM is soluble in water, possessing an isoelectric point ranging from 9.6 to 10.5 (Curtis et al., 2002; Fujita & Yoshikawa, 1999). Subsequently, the ≤3 kDa ultrafiltration (UF) fraction obtained from bonito fish underwent freeze-drying and was stored at temperatures below -18 ^{o}C in preparation for subsequent experiments.

3.2 Chitosan and Alginates Preparation

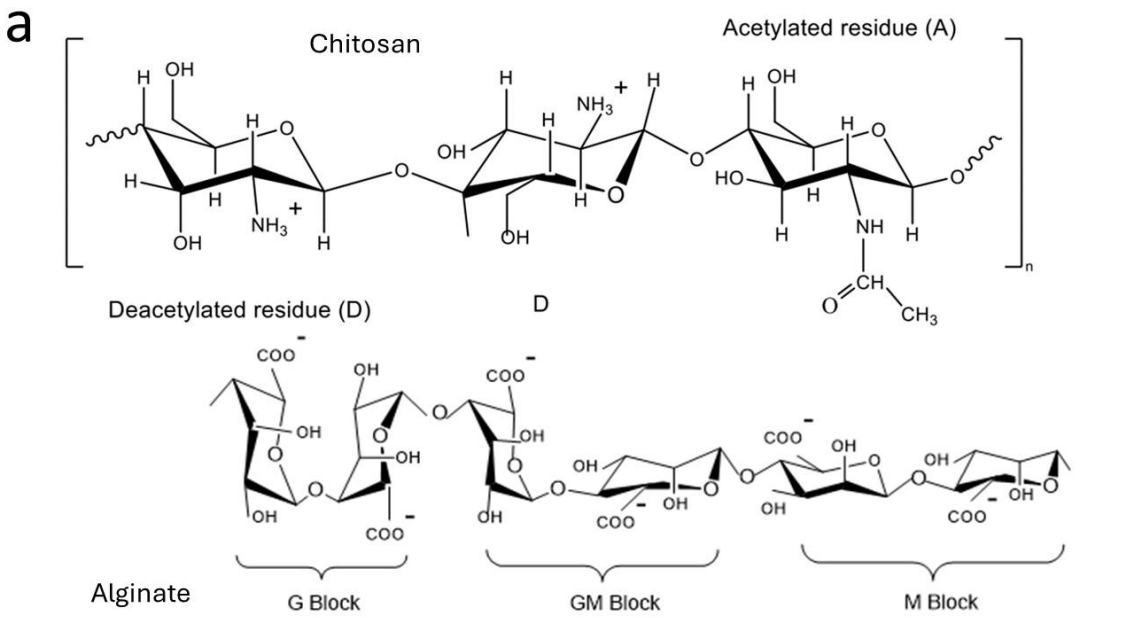

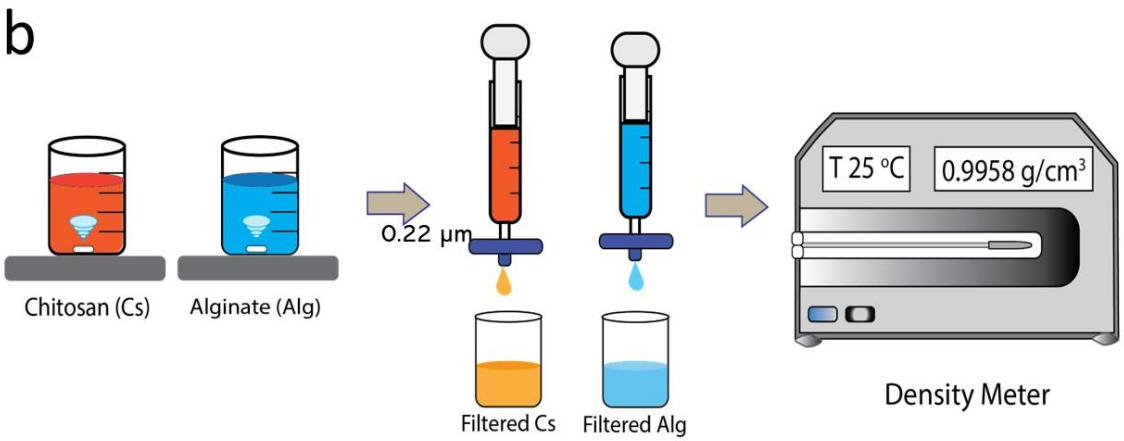

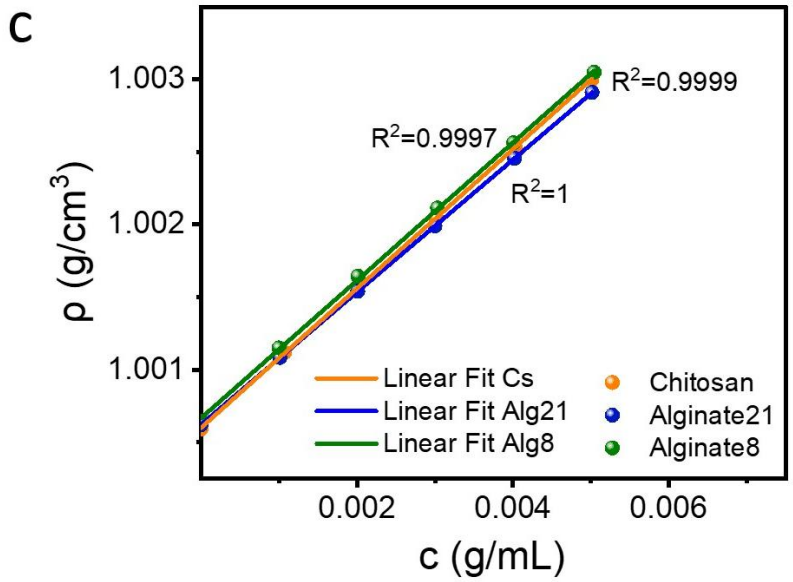

Figure 2. Chitosan/CS and alginate/ALG structures are shown (a). A schematic illustrates their stock solution preparation through filtration to remove aggregates and undissolved matter. Measurement is done using a density meter (b). Unfiltered CS and ALG standard curves (concentration/***c*** vs. density) aid precise post-filtration concentration estimation (c)

Chitosan (CS) was dissolved in a sodium chloride (NaCl), 85 mM concentration derived from a previous study that identified it as optimal for synthesizing CS-tripolyphosphate (TPP) nanocomplexes. To ensure consistency, alginate (ALG) was also dissolved in the same solvent at the same concentration. Both CS and ALG were set at a concentration of 2 mg/mL after filtration. Filtration of CS and ALG using a 0.22 µm membrane filter before complexation was deemed essential due to the potential aggregation of both polymers during solubilization. This filtration step served to separate any aggregates from the dissolved polymers. Additionally, filtration aided in capturing impurities such as dust or contaminants, ensuring the obtainment of pure biopolymer solutions. The elimination of impurities from the complex solution was particularly crucial for avoiding bias in hydrodynamic diameter (Rh) measurements using dynamic light scattering (DLS), a discussion of which will follow in the subsequent results section. Filtration is a commonly employed technique in the preparation of nanocomplexes, as demonstrated in studies by Sreekumar et al. (2022) for preparing stock solutions of CS and tripolyphosphate (TPP), as well as by Milkova and Goycoolea (2020) for establishing CS solutions with varying degrees of acetylation (DA) and molecular weight (M_w). However, it is noteworthy that the process of filtering CS and ALG may impact their final concentration. To address this, the density of both CS and ALG before filtration was measured to construct a

standard curve correlating concentration with density. Subsequently, concentration adjustments were made in certain instances using the filtered solvent to achieve comparable masses. Figure 2 illustrates the procedural steps involved in preparing CS and ALG solutions, measuring their density, and the resultant standard curve.

The determination of the actual concentrations of CS and ALG post-filtration was facilitated by employing a standard curve, establishing a linear correlation between the concentrations of biopolymers (in g/mL) and their corresponding densities (in g/cm³). The densities of both CS and ALG were quantified as the mass of these biopolymers within their respective volumes of solution. To ensure uniformity, the temperature was maintained at approximately 25°C, and the density meter was calibrated using the density of water at this temperature (ρ=0.997 g/cm³) as a reference point. The density of CS and ALG, both before and after filtration, was subsequently measured. The density of an 85 mM NaCl solution served as a representation of CS and ALG at a concentration of 0 mg/mL. In our preparations, CS with a Molecular Weight (M_w) of 110 kDa, and concentrations ranging from 0.1% to 0.5%, exhibited densities (ρ) within the range of 1.0012 to 1.0029 g/cm³. A comparable study conducted by Kumar et al. (2021), utilizing the same Anton Paar DMA-500 density meter, measured the densities of 0.75% (m/v) CS with high and medium M_w, recording values of 1.0012 and 1.0013 g/cm³, respectively. Kumar et al.'s study, however, did not provide specific details regarding the Mw of CS. For ALG, the density observed in our study did not significantly differ from that of CS, as depicted in Figure 2. Notably, ALG with a lower M_w (8 kDa) exhibited a slightly higher density compared to its counterpart with a higher M_w (21 kDa). While these distinctions may appear subtle, they are indeed discernible due to the remarkable sensitivity of the instrument. Based on the data obtained and the findings reported by Kumar et al. (2021), it can be generally asserted that lower M_w ALG or CS tends to possess slightly higher densities compared to their higher M_w counterparts. This observation aligns with the fundamental definition of density as the ratio of mass to volume, where volume represents the amount of space occupied by the material. Smaller materials are distributed more homogeneously throughout the entire solution.

3.3 Unloaded CS-ALG polyelectrolyte complexes (PECs)

Polyelectrolyte complexes (PECs) have been the subject of extensive research, serving as one of prominent method for encapsulating and delivering bioactive proteins and peptides

(Kulkarni et al., 2016). The formation of PECs involves the electrostatic interaction between a minimum of two oppositely charged molecules. In the context of CS-ALG PECs, these complexes arise through the ionic interaction between the cationic charged amino group (positive) of CS and the anionic charged carboxyl group (negative) of ALG. A critical parameter influencing PECs formation, stability, and encapsulation is the charge ratio (CR). However, there is a scarcity of published works focusing on tailoring the charge ratio in CS-ALG PECs formation. To the best of our knowledge, only the studies conducted by Sæther et al. (2008) and Yilmaz et al. (2019) have endeavored to control the CR in CS-ALG PECs formation. Both studies concur that as the CR approaches 1 (indicating an equilibrium of positive and negative charges), the electrostatic interaction intensifies, leading to the formation of coacervates or large aggregates, as opposed to excess CS or ALG. The zeta-potential of PECs in both studies exhibited high positive or negative values when there was an excess of CS or ALG, indicating implications for their stability.

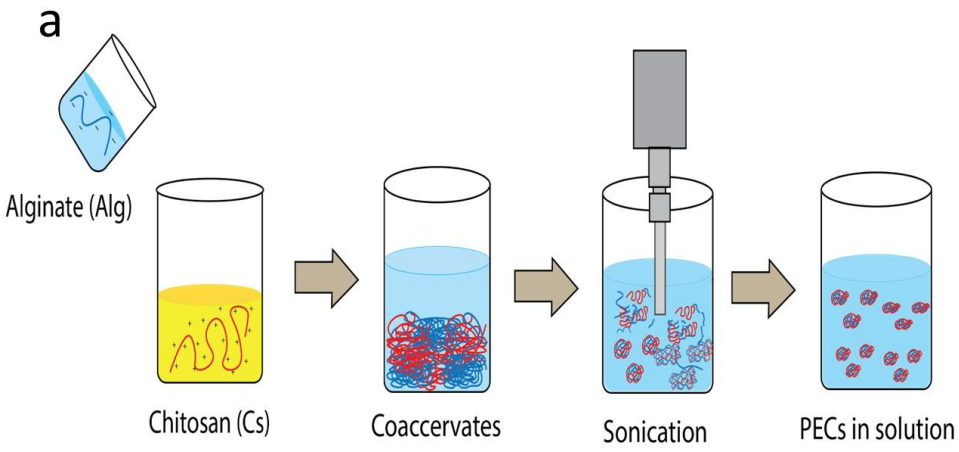

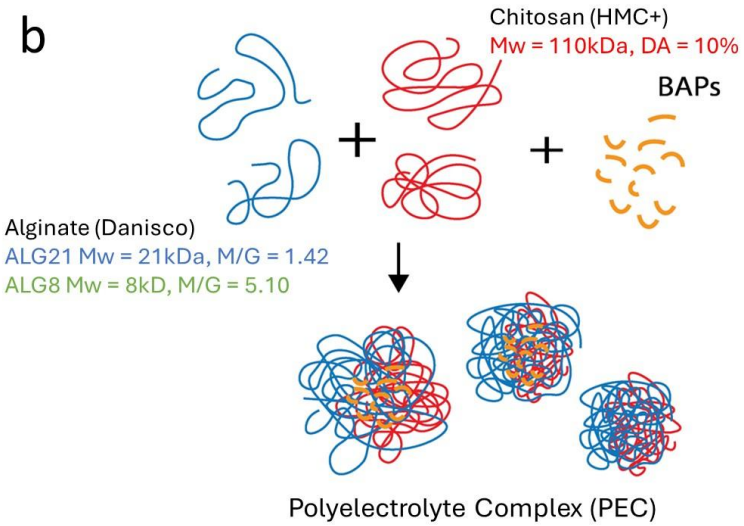

Figure 3. Schematics on how to prepare PECs via sonication (a) and complex formation (b)

3. 3.1 Size and zeta-potential

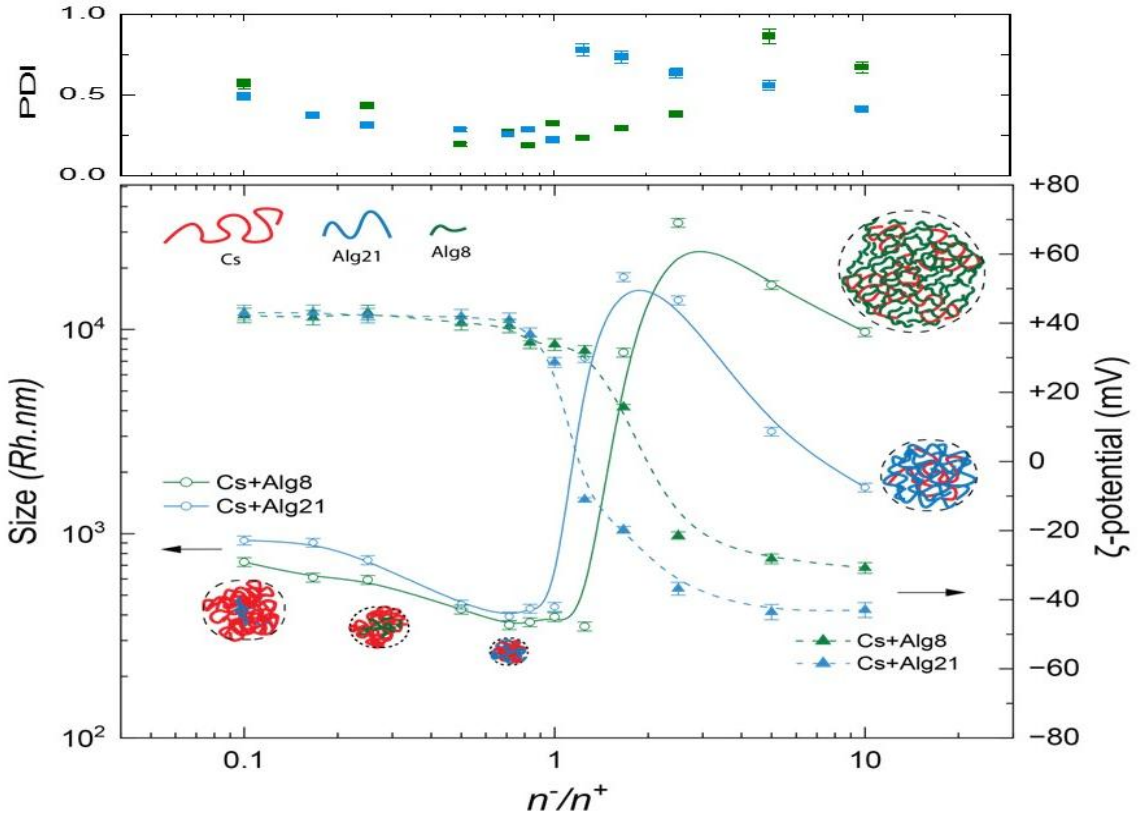

Figure 4. The variation of hydrodynamic size (R_h), zeta-potential, and PDI with molar charge ratio (n-/n+) of 'blank' (unloaded) CS/ALG PECs at a total polymer concentration of 2 mg/mL.

In our investigation, visual observations revealed a consistent trend in complex sizes, aligning with prior studies at a charge ratio (CR) near 1. This correspondence suggests a propensity for reduced charges through surface charge compensation, likely contributing to increased aggregation formation. Consequently, an additional treatment was introduced post-incubation, involving sonication (Figure 3), in accordance with findings from the study conducted by Saether et al. (2008). Their research indicated that homogenization aids in the breakdown of complex agglomerations, with an observed correlation between increased homogenization speed and smaller particle size of polyelectrolyte complexes (PECs). Notably, the study emphasized that larger dispersing element diameters during homogenization yield smaller particles. In our study, two low M_w variants of ALG (8 kDa and 21 kDa) were employed, with both CS (110 kDa) and ALG dissolved in a solution containing 85 mM sodium chloride (NaCl). This choice aligns with the findings of Goycoolea et al. (2009), who reported that smaller M_w of ALG result in smaller particles when combined with CS, and 85 mM NaCl serves as an optimal solution for generating complex nanoparticles (NPs). The hydrodynamic diameter (R_h) and zeta-potential of CS-ALG PECs at various CRs following sonication in our study are presented in Figure 4.

Figure 4 depicts the size and stability of CS-ALG PECs at charge ratios (CRs) ranging from 0.1 to 10. The size is characterized by the hydrodynamic radius (R_h), while stability is represented by the zeta-potential. In terms of R_h, the sizes of CS-ALG PECs decrease as the CR approaches 1, followed by a sharp and pronounced increase for CR >1 until 2.5. Subsequently, a decrease is observed as the CR approaches 10 (CR ALG ten times excess). However, this trend does not mirror the behavior observed at CR 0.1 (CR CS 10 times excess). The latter aligns with findings from Yilmaz et al. (2019), who reported that the R_h of CS-ALG PECs with ten times excess of CS exhibited a smaller diameter than those with ten times excess of ALG. Moreover, the R_h transition of PECs with excess CS is not as significant as the transition seen in PECs formed with excess ALG. This difference may be attributed to the polymer chain of CS being more prone to remaining straight before experiencing bending, indicated by a persistence length of 5 nm (Rinaudo et al., 1993; Schatz et al., 2004), while ALG tends to stay relatively straight and aligned for approximately 12 nm (Vold et al., 2006). Furthermore, the R_h of PECs formed with ALG M_w 21 kDa is slightly larger than those with ALG 8 kDa at CR <1. However, at CR >1, the R_h of PECs formed with ALG 8 kDa becomes significantly larger than their counterparts, indicating that excess CS contributes to robust

PECs. In terms of zeta-potential, excess CS imparts a high positive charge, while excess ALG generates a high negative charge in PECs, signifying that both surplus CS and ALG contribute to stable PECs. The surface charge of PECs from ALG 8 kDa and ALG 21 kDa is indistinguishable at CR <1. However, when excess ALG is mixed with CS, the PECs from ALG 21 kDa exhibit a higher negative zeta-potential. This suggests that ALG with a higher M_w exhibits an enhanced ability for charge compensation toward CS, owing to its superior ionic interaction ability. Therefore, when introduced into a system containing positively charged CS, the high M_w ALG effectively interacts with the positive charges. This result is further supported by Figure 5, which measures the viscosity of the supernatant from PECs after centrifugation which will discuss later. Centrifugation separates unassociated polymers in the supernatant, with higher viscosity indicating a greater proportion of unassociated ALG to CS or vice versa.

The results from figure 4 also depicted a complex dependence of PEC hydrodynamic radius (R_h) on n^-/n^+. For both ALGs at low n^-/n^+ (0.1 to 0.6), R_h steadily decreased slightly from ca. 800 to 300 ± 50 nm, indicating small, dense structures. The lower M_w ALG gave slightly smaller R_h. At $n^-/n^+ \sim 0.7$, i.e., just before overall charge neutralization ($n^-/n^+ =1$) R_h showed a sharp increase, rising to ca. 20 μm by $n^-/n^+ = 2$, followed a slower decrease in R_h to 10 and 2 μm as n^-/n^+ was raised further to 10 for ALG M_w's 8 and 21 kDa, respectively. Thus, the lower M_w ALG appeared to result in larger PECs at the higher n^-/n^+. It was also noticeable that dramatic increase in R_h appeared at a slightly lower n^-/n for the higher Mw ALG, suggesting the more 'efficient' cross-linking capacity of ALG Mw = 21 kDa compared to 8 kDa. This was also reflected in changes in the zeta (ζ)-potential as a function of n^-/n^+. As n^-/n^+ was raised, there was a smooth, sigmoidal transition from positively charged PECs (ζ= +43 ± 3 mV at $n^-/n^+ = 0.1$) to negatively charged PECs, but the higher Mw ALG resulted in ζ of greater magnitude: □ζ = -41 and -30 ± 3 mV at $n^-/n^+ = 10$ for ALG Mw 21 and 8 kDa, respectively. Also, the transition from positive to negative PECs was shifted to higher n^-/n^+ in the case of the 8 KDa ALG, indicating the greater difficulty of the lower M_w ALG in pulling the complexes together and completely coating them in ALG.

The polydispersity indexes (PDIs) of PECs derived from both ALGs exhibited analogous patterns, decreasing as the charge ratio (CR) approached 1, then increasing beyond CR>1, and subsequently decreasing again when CR reached 10. The escalation in PDIs at CR > 1 was more rapid for PECs formed with higher M_w ALG, suggesting a propensity for increased polydispersity.

3. 3.2 Complexation and molecular interaction

The investigation of complexation and molecular interactions between CS and ALG involved the measurement of their scattering patterns and viscosities. Viscosity (η) was determined using a microViscometer, while scattering patterns were analyzed through small angle X-scattering (SAXS). Following the mixing of CS and ALG stocks, the formation of coacervates was visibly evident; however, after sonication, the complexes in the solution became imperceptible to the naked eye. Consequently, η measurements in the supernatant were conducted after centrifugation, with the assumption that lower η indicates higher complexation. In other words, a reduction in η is attributed to the formation of complexes. Figure 5 illustrates the η of CS-ALG mixtures in the supernatant at varying ALG mass ratios, along with a theoretical additive line and the deviation from the additive line (additive viscosity). Figure 6 presents SAXS patterns and the corresponding Kratky plots both before and after complexation.

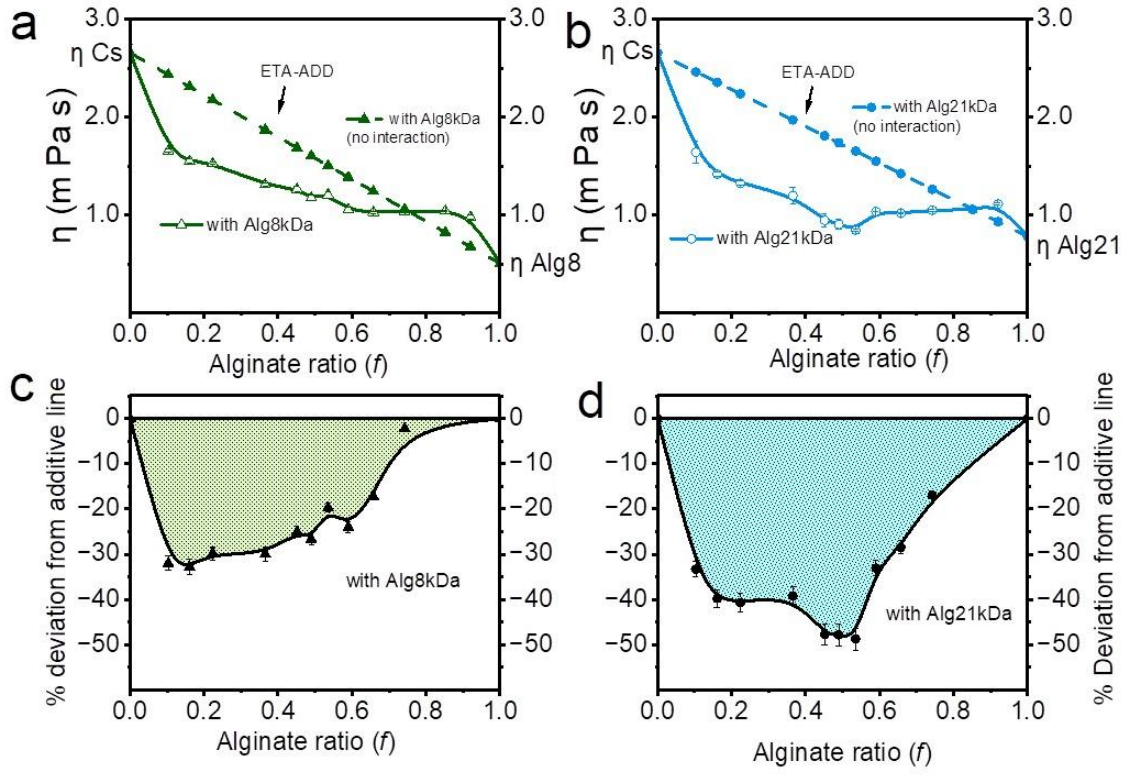

Figure 5. Viscosity (η) of CS-ALG mixtures of varying composition expressed as mass fraction of ALG (f) with respect to the total mass in CS-ALG 8 kDa (a), and CS-ALG 21 kDa (b) (25 ºC). The dash line in (a) and (b) represents the calculated values of η the mixtures assuming there is no interaction (additive line). The η values at f = 0 and 1 are the relative viscosities of the CS (2 mg/mL) and ALG (2 mg/mL) stock solution, respectively. The lower panels show the normalized data expressed as percentage deviation from the additive line in CS-ALG 8 kDa (c) and CS-ALG 21 kDa (d). The shaded areas in plots (c) and (d) represent the integrated area under the curve.

The amalgamation of a stock solution with an opposite charge to CS, at increasing mass proportions (f ratio, denoting the mass proportion of the CS counterpart relative to the total mixture mass), typically leads to a reduction in η to a minimum value (fηmin). Subsequently, upon further increasing f, the viscosity tends to rise, eventually approaching that of the counterpart stock solution (Menchicchi et al., 2014). However, in the present study, the dynamics were somewhat distinct, likely owing to the significantly smaller molecular weight (M_w) of ALG (more than 13 times smaller) compared to CS. In a single-step injection of ALG (Mw 8 kDa) into CS at f ratio 0.1 (10% ALG or 90% CS), the η sharply decreased, indicative of considerable η loss in CS and potential complex formation. Relative to this lowest f ratio, the η exhibited a slight decrease at f > 0.1 until 0.65, followed by an increase approaching the theoretical additive line (assuming no interaction, represented by the dashed line), until reaching the minimum η at f ~1, denoting 100% ALG 8 kDa. The η between f 0.7 and 1 were higher than the theoretical additive line, might be due to non-homogeneous mixing, where the η calculation considered only the solution saturated with CS-ALG complexes, while the η of pure ALG 8 kDa itself was exceptionally lower compared to the CS stock. Conversely, when mixing CS with ALG 21 kDa, the η in the supernatant sharply decreased, reaching a minimum at f ratio 0.53, indicative of maximum complexation. Subsequently, the η slightly increased, approaching the theoretical additive line at f ratio 0.85. At f ratio 0.92, the η was higher than the theoretical additive line, attributed to the consideration of only saturated CS-ALG complex solution. Figure 5a and 5b summarize that complexation with higher ALG Mw (21 kDa) likely occurred. This finding is supported by Figures 5c and 5d, which illustrate a skewed U-shaped curve describing the percent deviation from the additive line for CS complexation with ALG 21 kDa, deeper than that observed with ALG 8 kDa.

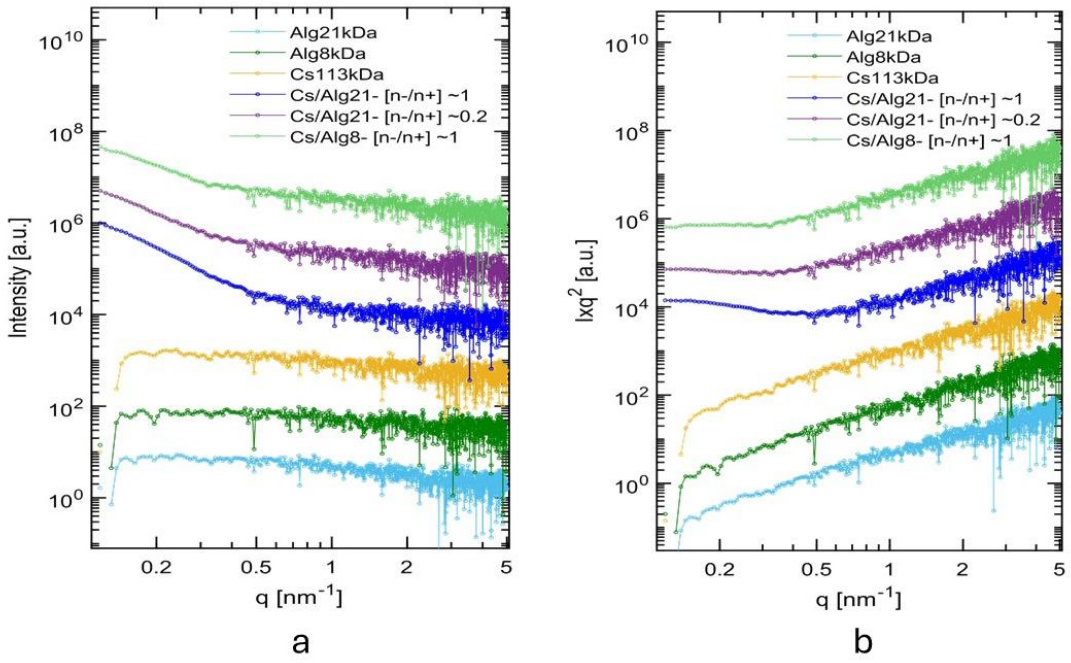

Figure 6. Small-angle X-ray scattering (SAXS) patterns (a) and corresponding Kratky plots (b) are presented for 2 mg/mL of CS, ALG, and their PECs at two different n-/n+ molar charge ratios. The Kratky plots demonstrate swollen chain behavior for pure polyelectrolytes, whereas Gaussian chain and 3D aggregates are observed for PECs (85 mM NaCl at 25 °C)

Figure 6 illustrates the scattering intensity of CS, ALG, and their complexation analyzed through small-angle X-scattering (SAXS). Figure 6a provides an overview of the scattering intensities for individual CS and ALG solutions, which exhibit plane scattering intensities from a scattering vector (q) of 0 to 5 nm, indicating homogeneous dissolution of biopolymers in the solution. In contrast, complexation of both biopolymers results in higher intensity compared to sole of CS and ALG, particularly at $q < 0.5$ nm, indicating a high electron density in the complexes. This high intensity at low q values suggests the creation of complex particles (Takeshita et al., 2019) and confirms the formation of CS-ALG complexes. Additionally, the higher intensity at low q values indicates the small size of CS-ALG complex particles, clearly in the nano and sub-micron dimensions. The CR for SAXS analysis was chosen at approximately 1 and 0.5, and the dynamic light scattering (DLS) analysis, as discussed earlier, confirmed the SAXS results, revealing that the hydrodynamic radius (R_h) of CS-ALG complexes at CR 1 is around 300 to <500 nm.

The Kratky plot (Figure 6b), which represents intensity × q^2 versus q, illustrates differences between individual CS or ALG biopolymers and their complexes. The single biopolymer solutions display a monotonous increasing behavior at higher q values, while the

CS-ALG complexes show an upward-sloping line with no clear peak, suggesting that the molecules are either flexible or structurally disordered. However, the moderately linear acceleration of the q style in both single and complex solutions indicates elongated chains with increased size due to swelling (Takeshita et al., 2019). In summary, the SAXS analysis of individual CS and ALG solutions and their complexation reveals a significant finding and three characteristic attributes. Firstly, the investigation unequivocally establishes that the mixing of two stocks of CS and ALG forms complexes distinct from the parent stock solutions, commonly referred to as polyelectrolyte complexes (PECs). Secondly, the size of these simple PECs fabrication is unrelated to the individual parent CS or ALG solutions, evident from distinct intensities at very low q values. Thirdly, the shape of PECs differs from the individual parent solutions (CS or ALG), as manifested by contrasting intensity styles at $q \leq 0.5$ nm. Moreover, the third aspect pertains to the internal structure, as there is no disparity observed between CS or ALG alone and their PECs. This is evidenced by an identical scattering pattern at higher q values (> 0.5 or > 1 nm) in both SAXS patterns and the Kratky plot, even though the models appear notably noisy. Consequently, it is concluded that there is no change in the internal structure of CS and ALG after complexation, suggesting they had interaction through ionic interaction and crosslinking.

3.4 Loaded CS-ALG PECs with short fish bioactive peptides (BAPs)

3. 4.1 Size, zeta-potential, and polydispersity

The PECs selected as vehicles for encapsulating short fish bioactive peptides (BAPs) were derived from CS mixed with ALG of 21 kDa. ALG 21 kDa was chosen for its clear propensity to form PECs with cationic CS over its counterpart (ALG 8 kDa), as evidenced by the resulting minimum additive η (Figure 5) and charge compensation (Figure 4) after complexation. However, at certain charge ratios (CR), the PECs from CS-ALG 21 kDa tended to be unstable in aqueous solution, as indicated by the zeta-potential in Figure 4 and visual observation. Therefore, specific CR values were chosen, namely CR 0.5 to represent excess CS and CR 10 to represent excess ALG. These representative CR values resulted in sub-micron-sized PECs, potentially enhancing the availability and solubility of the vehicles by improving the surface area and exhibiting more favorable stability, as expressed by zeta-potential values of around +40 mV or -40 mV (Figure 4).

The fractionated fish BAPs comprise two short BAPs, namely LKPNM and LKP, encapsulated using the selected CS-ALG CR through a one-step mixing technique of coacervation coupled with ultrasonication, as described for unloaded PECs preparation. The only distinction lies in the initial addition of the fish BAPs solution into the CS solution. Then the suspension contains two positively charged molecules, the CS and the peptides, where the short fish BAPs contain lysine that protonates across a wide range of pH levels. The suspension is then added to the ALG solution, followed by incubation for PEC formation and ultrasonication to tailor the coacervates and control the size.

The measurement of the hydrodynamic radius (R_h) of loaded and unloaded PECs was conducted using dynamic light scattering (DLS). It was observed that the R_h of loaded PECs is smaller compared to unloaded PECs, suggesting stronger complexation due to the presence of positively charged BAPs. This theory is supported by the significant reduction in size observed in the excess ALG PECs, indicating that the increased negative charge allows for stronger electrostatic attraction to the positive charges of BAPs and CS. Furthermore, the zeta-potential of loaded PECs with excess ALG also demonstrates a shift towards less negative values.

In contrast, when comparing unloaded and loaded PECs with excess CS, the reduction in R_h is not as substantial as with excess ALG, and the reduction in zeta-potential is negligible. As previously mentioned, the R_h of PECs with excess CS is lower than that of PECs with excess ALG. Table 1 presents the R_h, zeta-potential, and polydispersity index (PDI) of unloaded and loaded PECs. Regarding PDI, there is a tendency toward monodispersity when there is an excess of CS, while an excess of ALG leans more toward polydispersity. A PDI score between 0 and 0.1 indicates monodispersity, suggesting highly uniform particle sizes (Raval et al., 2019). A PDI between 0.1 and 0.3 suggests moderate polydispersity with a somewhat broader size range but still relatively uniform (Gazzillo et al., 2006). When the PDI is between 0.3 and 1.0, or greater than 0.7, it signifies a diverse range of particle sizes, indicating a mixture with significant variations (Mudalige et al., 2019).

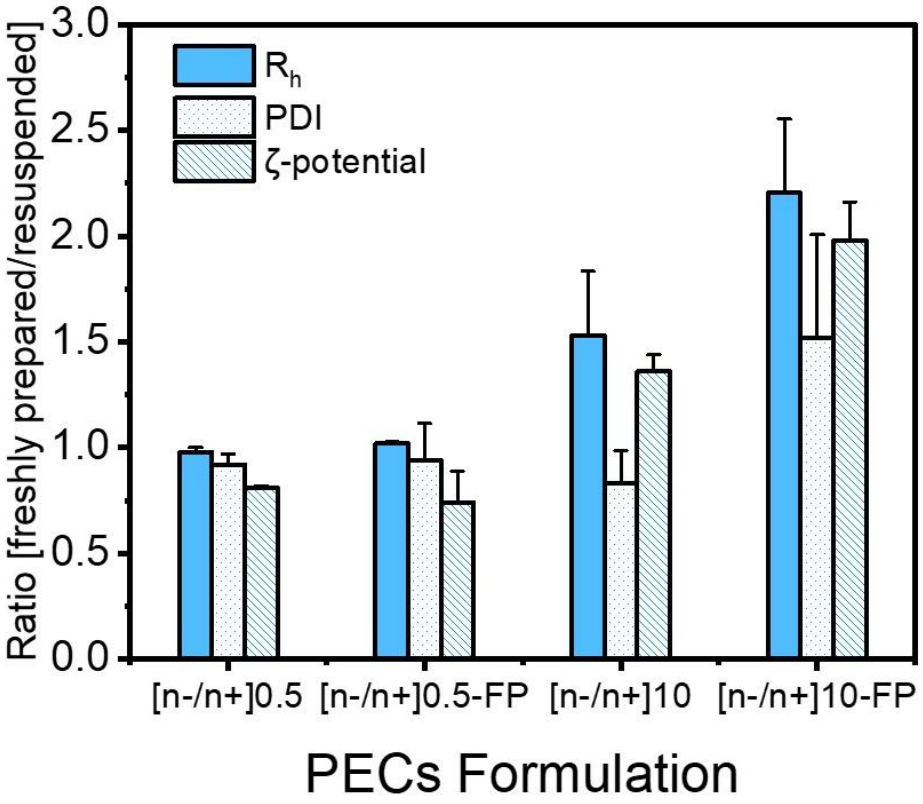

Figure 7. Comparison of the ratio of R_h, polydispersity index (PDI), and zeta-potential between non-resuspended (freshly prepared) PECs and resuspended PECs (with 500 µL 85 mM NaCl), both loaded (FP) and unloaded (NOP) with excess CS [n-/n+] 0.5 and excess ALG [n-/n+] 10

We also investigated the influence of resuspension on the R_h, zeta-potential, and polydispersity index (PDI) of both loaded and unloaded PECs. As shown in Figure 7, the ratio between freshly prepared and resuspended PECs with excess CS was around 1.0 or close to 1.0, indicating no significant differences. In other words, resuspension did not alter the size, zeta-potential, and PDI of PECs in this formulation. However, in the case of PECs with excess ALG, we observed that the ratio was higher than 1.0, particularly for R_h and zeta-potential, indicating that resuspension of PECs with excess ALG reduced their R_h and zeta-potential. This suggests that a significant amount of ALG was lost during resuspension, and the ALG that was supposed to be in the outer loops of complexes was not strongly bound. Therefore, it was easily discharged into the supernatant.

3. 4.2 Encapsulation efficiency (EE) and yield

The encapsulation efficiency (EE) of BAPs is critical as it is associated with optimal dosing and maximum therapeutic benefits. In the context of consumption, the widely accepted consensus is that achieving the maximum desired function with minimal dosing is the ultimate goal. The EE of short fish BAPs was quantified by comparing the concentration of initially added BAPs to the BAPs encapsulated within PECs. In this study, the concentration of remaining BAPs in the supernatant after complexation was used to calculate the amount of unencapsulated BAPs. The results revealed that the EE of short fish BAPs into CS-ALG PECs was 80.6% (excess ALG) and 85% (excess CS). Previous studies have attempted to encapsulate short BAPs through ionic gelation or coacervation. For example, a study by Danish et al. (2017) reported an EE between 22.6% and 43.9% for the encapsulation of IPP and around 40.9% to 65.1% for the encapsulation of LKP, both into CS nanoparticles (NPs). The EE of tripeptide YKT into CS macroparticles (MP) was approximately 35% (Bicak et al., 2021). Encapsulation of the decapeptide YLGYLEQLLR into guar-gum, then coated with CS MPs, yielded an EE of about 86%. These results suggest that creating composites with at least two biopolymers electrostatically enables an increase in EE. The yield (%) of PECs before and after complexation with BAPs also indicates that the BAPs form a complex, as evidenced by an increase in yield after adding short fish BAPs. The yield is higher in PECs with excess CS, indicating a larger amount of complexation and BAPs encapsulated in this formulation compared to excess ALG. This finding reinforces the outcomes presented and discussed in the sections above. Table 1 also presents the EE of fish BAPs into PECs and their yield.

Table 1. Selected PEC systems CS-ALG with and without fish bioactive peptides loading

System	[n-/n+]	Rh (nm)	PDI	ζ-potential (mV)	Encapsulation Efficiency (EE) (%)	Yield (%)
PECs CS-ALG Blank	0.5	402±13^{a}	0.248±0.02^{a}	+36.0±2.1^{a}	-	8.63±0.71^{bc}
	10	843±88^{b}	0.493±0.06^{b}	-23±1.3^{c}	-	3.04±1.41^{c}
PECs CS-ALG-Peptide	0.5	322±2^{a}	0.191±0.008^{a}	+33.9±1.3^{b}	85±0.08	13.5±1.14^{ab}
	10	436±54^{a}	0.417±0.04^{b}	-14.6±2.3^{d}	80.6±0.5	6.93±5.79^{bc}

- Symbols in the same column with different notations indicate differences with significance >95% ($p < 0.05$).

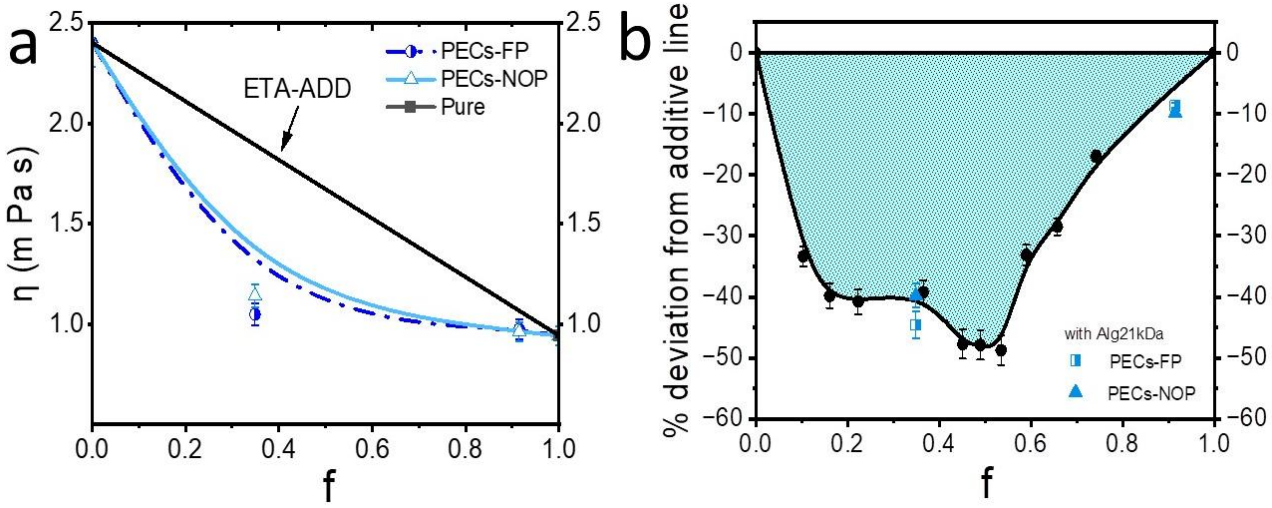

Figure 8. Viscosity (η) of CS-ALG 21kDa both loaded (blue) and unloaded (light blue), the mixtures of composition expressed as mass fraction of ALG (f) with respect to the total mass in (25 °C) (a). The solid line (black) represents the calculated values of η the mixtures assuming there is no interaction (additive line). The η values at f = 0 and 1 are the relative viscosities of the CS (2 mg/mL) and ALG (2 mg/mL) stock solution, respectively. The panel show the normalized data expressed as percentage deviation from the additive line in CS-ALG 21 kDa, loaded (square) and unloaded (triangle) compared with initial data of unloaded CS-ALG21 kDa, the shaded area in plot represents the integrated area under the curve (b).

To corroborate these discoveries, we also measured the viscosity (η) of the supernatant of loaded PECs and unloaded PECs with excess CS and excess ALG. The results indeed showed that the η of loaded PECs in the supernatant was lower than that of unloaded PECs, especially with excess CS (Figure 8a). This observation is further emphasized by the percent deviation from the additive line depicted in Figure 8b. Typically, the η is significantly lower when compared to the additive line (indicating no interaction), particularly with excess CS, suggesting a higher degree of complexation. This trend is also supported by Figure 8b.

3. 4.3 Morphology

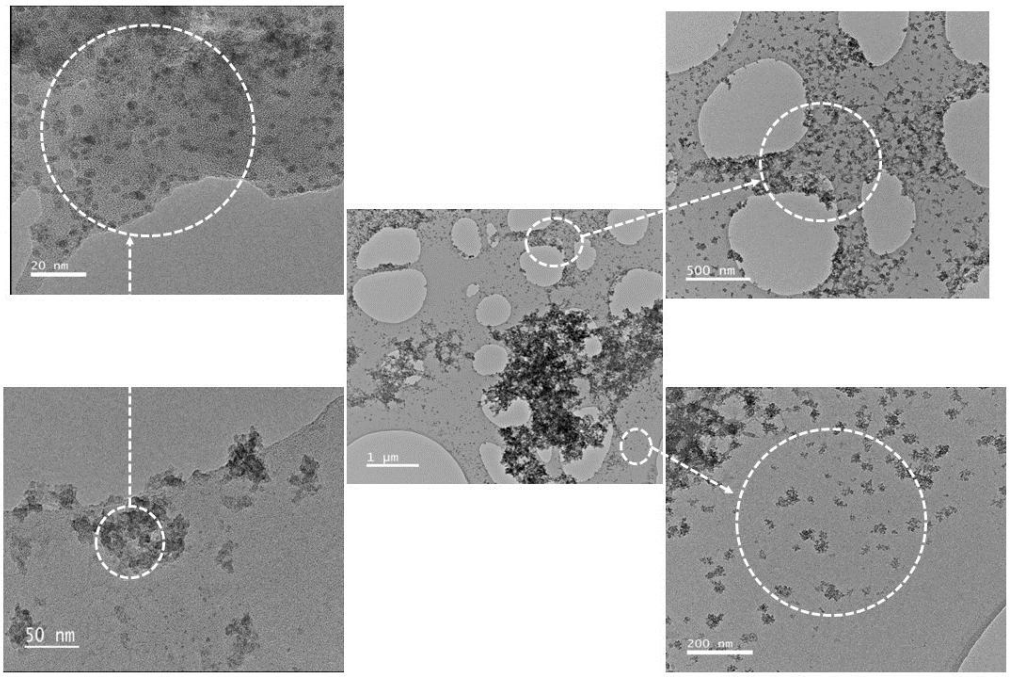

Figure 9. Transmission Electron Microscopy (TEM) images display PECs loaded with fish peptides at an excess CS [n-/n+] 0.5 (PECs-0.5-FP). Analysis was performed using a FEI Titan3 Themis G2 S/TEM at 300 kV with a Gatan OneView 4K CMOS camera. Magnifications are indicated in the scale bars.

The morphology of the carrier agent for BAPs was examined through transmission electron microscopy (TEM). The analysis focused on the loaded PECs with excess CS (figure 9), as this complex appeared more robust and exhibited a higher encapsulation efficiency (EE). Although the size, represented by the hydrodynamic radius (R_h) of the loaded PECs analyzed via dynamic light scattering (DLS), was approximately 322 nm with a polydispersity index of 0.191, TEM images revealed a different perspective on the diameter. The TEM images showcased polydisperse particles ranging from less than 20 nm to over 500 nm, with some larger particles exceeding 1 µm, indicating aggregation. It is important to note that while DLS and TEM are both analytical techniques for characterizing submicron and nanomaterials, they have inherent differences. DLS, also known as Photon Correlation Spectroscopy (PCS), measures the Brownian motion of particles within a solution, with smaller particles exhibiting faster fluctuations. The R_h is obtained using the Stokes-Einstein equation, relating particle movement to the diffusion coefficient. On the other hand, TEM is a high-resolution microscopy technique that utilizes electrons, rather than light, to visualize nanomaterials. It achieves high

magnification by adjusting electromagnetic lenses. Encapsulation of tripeptides LKP and IPP separately with CS yielded diameters around 113 to 209 nm and 125 to 207 nm, respectively. In contrast, the encapsulation of the pentapeptide VLPVP with a composite of two polymers, carboxymethyl CS/Na-ALG, resulted in microsphere vehicles with diameters ranging from 5.4 to 43.8 μm.

The morphology of the PECs reveals round shapes for smaller diameters (< 20 nm) and a more spherical configuration for larger diameters (< 500 nm), indicating a tendency for spherical particles to agglomerate and form micro and macro-size complexes. This observation aligns with reported findings in BAPs-loaded nanoparticles (NPs) and microparticles (MPs), where a regular spherical morphology is evident, whether in liposomes coated with Lactobacillus S-layer protein, sodium alginate-O-carboxymethyl CS microspheres, or Eudragit-coated CS NPs (Chen et al., 2017; Huang et al., 2017; Jiang et al., 2021). The investigation of small particle shapes often utilizes techniques such as transmission electron microscopy (TEM), scanning electron microscopy (SEM), and atomic force microscopy (AFM). Huang et al. (2017) focused on pentapeptide VLPVP-loaded sodium ALG-O-carboxymethyl CS microspheres, noting that the surface of the microspheres appeared rough, becoming smoother as membrane pore size increased to 5 μm or higher, depending on the encapsulation technique. Additionally, studies on CS nanoparticles loaded with tripeptide YKT revealed a solid and dense structure (Bicak et al., 2021).

3.4.4 Release study

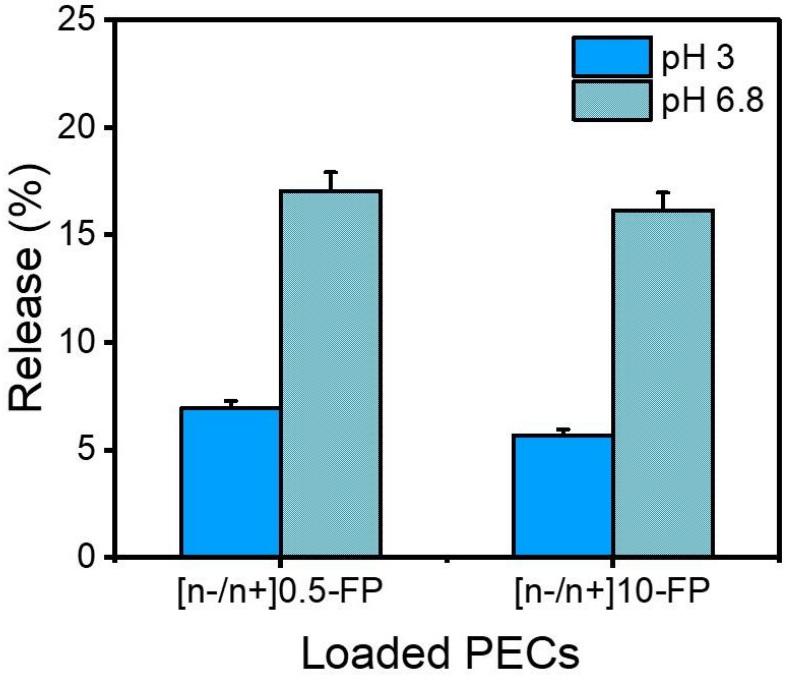

Figure 10. The release of fish peptides from PECs CS-ALG 21 kDa under conditions of excess CS [n-/n+] 0.5 (PECs-0.5-FP) and excess ALG [n-/n+] 10 (PECs-0.5-FP) after a 3-hour incubation at room temperature, at both pH 3 and pH 6.8. The quantification of fish peptide release was conducted using RP-HPLC UV/Vis.

The release of BAPs from carriers is commonly assessed by incubating BAPs-loaded vehicles in physiological solutions, with or without enzymes, mimicking gastric and intestinal conditions. Typically, the mixture is placed in a dialysis bag within a buffer and incubated. At specific intervals, buffer samples are withdrawn, and BAP concentrations are quantified using HPLC-UV detection or a spectrophotometer assay (Batista et al., 2021; Danish et al., 2017; Zhang et al., 2019). Some studies were not to use dialysis bags, instead directly withdrawing physiological solution after incubation, followed by centrifugation and subsequent BAP concentration analysis in the supernatant (Huang et al., 2017; Stephansen et al., 2014).

In our study, we investigated BAP release from PECs by incubating loaded PECs in solutions at both room temperature and pH 3 (representative of gastric acidity) and pH 6.8 (representative of intestinal conditions without enzymes). After 3 hours, the simulated pH suspension was centrifuged, and the amount of released BAPs in the supernatant was quantified using reverse-phase high-performance liquid chromatography (RP-HPLC). The results

indicated that BAP release was less than 8% at pH 3 and less than 18% at pH 6.8. The higher release of BAPs at pH 6.8 compared to lower pH can be attributed to the pH-dependent charge states of CS and ALG. At low pH (such as pH 3), CS carries a positive charge due to the protonation of amino groups, leading to stronger interactions and reduced BAP release. Conversely, at high pH (above the isoelectric point), CS loses its positive charge due to deprotonation, resulting in weakened ionic interactions with oppositely charged ALG, ultimately facilitating the release of a substantial quantity of BAPs from the complexes. Figure 10 presents the release of fish BAPs at two different pH.

In comparison to previous studies, the release of short-chain BAPs during gastrointestinal simulation is a common observation across various types of reviewed carrier agents. The release kinetics tend to be mitigated when utilizing composited or hybrid wall materials. For instance, the tripeptide ECG loaded into CS/β-cyclodextrin (β-CD) nanoparticles exhibited a release of 100% and ~25% after 200 minutes of incubation at pH 1.2 and pH 6.8, respectively. A similar tripeptide loaded into CS/α-cyclodextrin (α-CD) released approximately 60% before 200 minutes and 100% from CS/SBE-β-cyclodextrin at <100 minutes (Trapani et al., 2010). When the dipeptide FW was loaded into whey microbeads, it demonstrated a release of 56% after 6 hours of incubation, and when the volume ratio of microbeads to peptide (Vbead:Vaq) was <0.2, the release reached around 80% (O'Neill et al., 2015). Additionally, the pentapeptide VLPVP encapsulated within O-carboxymethyl CS/sodium ALG microspheres released 9.59% (pH 1.2, 2 hours) and 87.63% (pH 6.8, 5 hours) (Huang et al., 2017). Guar film-coated CS microparticles effectively protected the decapeptide YLGYLEQLLR, exhibiting only <2.5% release after 4 hours, with the study utilizing artificial saliva (Batista et al., 2021).

In another study, tripeptides IPP and LKP loaded into CS nanoparticles demonstrated releases of up to 90% in simulated intestinal fluid (SIF) after 240 minutes of incubation and approximately 75% after 120 minutes in simulated gastric fluid (SGF). These peptides released more than 60% within the first two hours of incubation in acidic simulation fluids (Danish et al., 2017). Similarly, the tripeptide YKT loaded into CS nanoparticles showed releases of 26%, 34%, 43%, and 97% after 8, 24, 48, and 264 hours of incubation, respectively. The release kinetics were lower in CS-ALG nanoparticles; for example, the tripeptide KPV encapsulated into CS/ALG nanoparticles released about 25% at pH 6.2 within 30 minutes, with the release kinetics remaining linear at 35% until 30 hours (Laroui et al., 2010; Xiao et al., 2017).

IV. CONCLUSION

This study has shown the robust structural integrity of CS-ALG polymeric electrolyte complexes (PECs) at a charge ratio (CR) below 1. Enhanced stability is observed in PECs with both excess CS and excess ALG in a NaCl solution, as evidenced by their zeta-potential. In comparison, the ionic interaction between CS and ALG of 21 kDa is more pronounced, resulting in a more intricate complexation compared to CS and ALG of 8 kDa. The introduction of short fish bioactive peptides (BAPs) into CS-ALG PECs leads to a reduction in hydrodynamic radius (R_h), with minimal impact on stability (zeta-potential) and dispersity. This size reduction, indicative of successful complexation of bioactives, is further supported by a decrease in viscosity (η) in the supernatant and an increase in yield. The encapsulation efficiency (EE) of BAPs in PECs with excess CS slightly surpasses that in PECs with excess ALG. Additionally, PECs with excess CS exhibit consistent biophysical properties (R_h, zeta-potential, PDI index) between freshly prepared and resuspended forms, suggesting minimal dissociation of molecules post-complexation. Moreover, the release of fish BAPs from CS-ALG PECs is higher at intestinal pH compared to gastric pH. Thus, this one-step mixing PECs system presents a promising encapsulation technique for future industrial development, offering a sustainable approach for incorporating BAPs into gastrointestinal delivery vehicles.

REFERENCES

Abdelhedi, O., Nasri, R., Mora, L., Toldrá, F., Nasri, M., & Jridi, M. (2017). Collagenous proteins from black-barred halfbeak skin as a source of gelatin and bioactive peptides. *Food Hydrocolloids, 70*, 123-133. https://doi.org/10.1016/j.foodhyd.2017.03.030

Aguilar-Toala, J. E., Quintanar-Guerrero, D., Liceaga, A. M., & Zambrano-Zaragoza, M. L. (2022, Feb 22). Encapsulation of bioactive peptides: a strategy to improve the stability, protect the nutraceutical bioactivity and support their food applications. *RSC Adv, 12*(11), 6449-6458. https://doi.org/10.1039/d1ra08590e

Alonso, M. J., & Goycoolea, F. M. (2008). Chitosan-polysaccharide blended nanoparticles for controlled drug delivery. In N. M. Neves, J. F. Mano, M. E. Gomes, A. P. Marques, & H. S. Azevedo (Eds.), *Natural-based polymers for biomedical applications* (pp. 644-679). Woadhead Publishing Ltd.

Apostolidis, E., Stergiou, A., Kioupis, D., Sadeghpour, A., Paximada, P., Kakali, G., & Mandala, I. (2023). Production of nanoparticles from resistant starch via a simple three-step physical treatment. *Food Hydrocolloids, 137*. https://doi.org/10.1016/j.foodhyd.2022.108412

Basirico, L., Catalani, E., Morera, P., Cattaneo, S., Stuknyte, M., Bernabucci, U., De Noni, I., & Nardone, A. (2015, Nov). Release of angiotensin converting enzyme-inhibitor peptides during in vitro gastrointestinal digestion of Parmigiano Reggiano PDO cheese and their absorption through an in vitro model of intestinal epithelium. *J Dairy Sci, 98*(11), 7595-7601. https://doi.org/10.3168/jds.2015-9801

Batista, P., Castro, P. M., Madureira, A. R., Sarmento, B., & Pintado, M. (2021). Preparation, characterization and evaluation of guar films impregnated with relaxing peptide loaded into chitosan microparticles [Article]. *Applied Sciences (Switzerland), 11*(21), Article 9849. https://doi.org/10.3390/app11219849

Bicak, B., Budama-Kilinc, Y., Kecel-Gunduz, S., Zorlud, T., & Akman, G. (2021). Peptide based nano-drug candidate for cancer treatment: Preparation, characterization, in vitro and in silico evaluation. *Journal of Molecular Structure, 1240*. https://doi.org/10.1016/j.molstruc.2021.130573

Cao, S., Wang, Y., Hao, Y., Zhang, W., & Zhou, G. (2020, Jan 22). Antihypertensive effects in vitro and in vivo of novel angiotensin-converting enzyme inhibitory peptides from bovine bone gelatin hydrolysate. *J Agric Food Chem, 68*(3), 759-768. https://doi.org/10.1021/acs.jafc.9b05618

Cazorla-Luna, R., Martin-Illana, A., Notario-Perez, F., Ruiz-Caro, R., & Veiga, M. D. (2021, Jul 8). Naturally occurring polyelectrolytes and their use for the development of

complex-based mucoadhesive drug delivery systems: an overview. *Polymers (Basel), 13*(14). https://doi.org/10.3390/polym13142241

Cermeño, M., Kleekayai, T., Amigo-Benavent, M., Harnedy-Rothwell, P., & FitzGerald, R. J. (2020). Current knowledge on the extraction, purification, identification, and validation of bioactive peptides from seaweed. *Electrophoresis, 41*(20), 1694-1717. https://doi.org/10.1002/elps.202000153

Chen, S. X., Guo, F., Deng, T. T., Zhu, S. Q., Liu, W. Y., Zhong, H. J., Yu, H., Luo, R., & Deng, Z. Y. (2017, May). Eudragit S100-coated chitosan nanoparticles co-loading Tat for enhanced oral colon absorption of insulin. *Aaps Pharmscitech, 18*(4), 1277-1287. https://doi.org/10.1208/s12249-016-0594-z

Curtis, J. M., Dennis, D., Waddell, D. S., MacGillivray, T., & Ewart, H. S. (2002). Determination of angiotensin-converting enzyme inhibitory peptide Leu-Lys-Pro-Asn-Met (LKPNM) in bonito muscle hydrolysates by LC−MS/MS [Original Article]. *Journal of Agricultural and Food Chemistry, 50*, 3919−3925. https://doi.org/https://doi.org/10.1021/jf011684c

Danish, M. K., Vozza, G., Byrne, H. J., Frias, J. M., & Ryan, S. M. (2017, Dec). Comparative study of the structural and physicochemical properties of two food derived antihypertensive tri-peptides, Isoleucine-Proline-Proline and Leucine-Lysine-Proline encapsulated into a chitosan based nanoparticle system. *Innovative Food Science & Emerging Technologies, 44*, 139-148. https://doi.org/10.1016/j.ifset.2017.07.002

Doroszkowski, A. (1999). The physical chemistry of dispersion. In R. Lambourne & T. A. Strivens (Eds.), *Paint and Surface Coatings: Theory and Practice* (Second Edition ed., pp. 198-242). Woodhead Publishing Limited.

Estévez, N., Fuciños, P., Fuciños, C., Jauregi, P., Tovar, C. A., & Rúa, M. L. (2020). Hydrolysis of whey protein as a useful approach to obtain bioactive peptides and a β-Lg fraction with different biotechnological applications. *Food Hydrocolloids, 109*. https://doi.org/10.1016/j.foodhyd.2020.106095

Feng, K., Li, C., Wei, Y. S., Zong, M. H., Wu, H., & Han, S. Y. (2019, Sep). Development of a polysaccharide based multi-unit nanofiber mat for colon-targeted sustained release of salmon calcitonin. *Journal of Colloid and Interface Science, 552*, 186-195. https://doi.org/10.1016/j.jcis.2019.05.037

Fernández-Musoles, R., Salom, J. B., Castelló-Ruiz, M., Contreras, M. d. M., Recio, I., & Manzanares, P. (2013). Bioavailability of antihypertensive lactoferricin B-derived peptides: transepithelial transport and resistance to intestinal and plasma peptidases. *International Dairy Journal, 32*(2), 169-174. https://doi.org/10.1016/j.idairyj.2013.05.009

Fuentea, B. d. l., Tornosa, A., Príncepa, A., Lorenzob, J. M., Pateirob, M., Berradaa, H., Barbaa, F. J., Ruiza, M.-J., & Martí-Quijal, F. J. (2020). Scaling-up processes: Patents and commercial applications. In J. M. Lorenzo & F. J. Barba (Eds.), *Aquaculture and By-Products: Challenges and Opportunities in the Use of Alternative Protein Sources and Bioactive Compounds* (Vol. 92, pp. 187-223). Academic Press. https://doi.org/https://doi.org/10.1016/bs.afnr.2019.12.003

Fujita, H., Yokoyama, K., & Yoshikawa, M. (2000). Classification and antihypertensive activity of angiotensin I-converting enzyme inhibitory peptides derived from food proteins. *Journal of Food Science, 65*(4), 564-569.

Fujita, H., & Yoshikawa, M. (1999). LKPNM: a prodrug-type ACE-inhibitory peptide derived from fish protein. *Immunopharmacology, 44*, 123–127. https://doi.org/10.1016/s0162-3109(99)00118-6

Gao, R., Yu, Q., Shen, Y., Chu, Q., Chen, G., Fen, S., Yang, M., Yuan, L., McClements, D. J., & Sun, Q. (2021). Production, bioactive properties, and potential applications of fish protein hydrolysates: Developments and challenges. *Trends in Food Science & Technology, 110*, 687-699. https://doi.org/10.1016/j.tifs.2021.02.031

Gazzillo, D., Fantoni, R., & Giacometti, A. (2006). Phase behaviour of polydisperse sticky hard spheres: analytical solutions and perturbation theory. *Molecular Physics, 104*(22-24), 3451-3459. https://doi.org/10.1080/00268970601050892

George, M., & Abraham, T. E. (2006, Aug 10). Polyionic hydrocolloids for the intestinal delivery of protein drugs: alginate and chitosan--a review. *J Control Release, 114*(1), 1-14. https://doi.org/10.1016/j.jconrel.2006.04.017

Gombotz, W. R., & Wee, S. F. (1998). Protein release from alginate matrices. *Advanced Drug Delivery Reviews, 31*, 267–285.

Goycoolea, F. M., Lollo, G., Remunan-Lopez, C., Quaglia, F., & Alonso, M. J. (2009). Chitosan-alginate blended nanoparticles as carriers for the transmucosal delivery of macromolecules. *Biomacromolecules, 10*, 1736–1743. https://doi.org/https://doi.org/10.1021/bm9001377

Guan, Z., Tjoeng, F. S., Li, W., Mandrell, K., Liu, M., & Chen, X. (2001). *Anti-hypertensive Peptides* (United States Patent No. W. I. P. Organization.

Guo, Q., Chen, P., & Chen, X. (2023). Bioactive peptides derived from fermented foods: preparation and biological activities. *Journal of Functional Foods, 101*. https://doi.org/10.1016/j.jff.2023.105422

Halim, N. R. A., Yusof, H. M., & Sarbon, N. M. (2016). Functional and bioactive properties of fish protein hydolysates and peptides: A comprehensive review. *Trends in Food Science & Technology, 51*, 24-33. https://doi.org/10.1016/j.tifs.2016.02.007

Han, R., Hernandez Alvarez, A. J., Maycock, J., Murray, B. S., & Boesch, C. (2021). Comparison of alcalase- and pepsin-treated oilseed protein hydrolysates - Experimental validation of predicted antioxidant, antihypertensive and antidiabetic properties. *Curr Res Food Sci, 4*, 141-149. https://doi.org/10.1016/j.crfs.2021.03.001

Han, R., Maycock, J., Murray, B. S., & Boesch, C. (2019, Jan). Identification of angiotensin converting enzyme and dipeptidyl peptidase-IV inhibitory peptides derived from oilseed proteins using two integrated bioinformatic approaches. *Food Res Int, 115*, 283-291. https://doi.org/10.1016/j.foodres.2018.12.015

Harnedy, P. A., O'Keeffe, M. B., & FitzGerald, R. J. (2017, Oct). Fractionation and identification of antioxidant peptides from an enzymatically hydrolysed Palmaria palmata protein isolate. *Food Res Int, 100*(Pt 1), 416-422. https://doi.org/10.1016/j.foodres.2017.07.037

Hayes, M., & Tiwari, B. K. (2015). Bioactive carbohydrates and peptides in foods: an overview of sources, downstream processing steps and associated bioactivities. *International Journal of Molecular Sciences, 16*, 22485-22508. https://doi.org/10.3390/ijms160922485

Huang, G.-Q., Xiao, J.-X., Hao, L.-Q., & Yang, J. (2017). Microencapsulation of an angiotensin I-converting enzyme inhibitory peptide VLPVP by membrane emulsification. *Food and Bioprocess Technology, 10*(11), 2005-2012. https://doi.org/10.1007/s11947-017-1953-9

Jiang, B., Zhang, X., Yuan, Y., Qu, Y., & Feng, Z. (2017, Oct 17). Separation of antioxidant peptides from pepsin hydrolysate of whey protein isolate by ATPS of EOPO co-polymer (UCON)/phosphate. *Sci Rep, 7*(1), 13320. https://doi.org/10.1038/s41598-017-13507-9

Jiang, X. X., Pan, D. D., Tao, M. X., Zhang, T., Zeng, X. Q., Wu, Z., & Guo, Y. X. (2021, Jul). New nanocarrier system for liposomes coated with Lactobacillus acidophilus S-layer protein to improve Leu-Gln-Pro-Glu absorption through the intestinal epithelium. *Journal of Agricultural and Food Chemistry, 69*(27), 7593-7602. https://doi.org/10.1021/acs.jafc.1c01498

Kulkarni, A. D., Vanjari, Y. H., Sancheti, K. H., Patel, H. M., Belgamwar, V. S., Surana, S. J., & Pardeshi, C. V. (2016, Nov). Polyelectrolyte complexes: mechanisms, critical experimental aspects, and applications. *Artif Cells Nanomed Biotechnol, 44*(7), 1615-1625. https://doi.org/10.3109/21691401.2015.1129624

Kumar, M., Hasan, M., Choyal, P., Tomar, M., Gupta, O. P., Sasi, M., Changan, S., Lorenzo, J. M., Singh, S., Sampathrajan, V., Dhumal, S., Pandiselvam, R., Sharma, K., Satankar, V., Waghmare, R., Senapathy, M., Sayed, A. A. S., Radha, Dey, A., Amarowicz, R., & Kennedy, J. F. (2022). Cottonseed feedstock as a source of plant-based protein and bioactive peptides: Evidence based on biofunctionalities and industrial applications. *Food Hydrocolloids, 131*. https://doi.org/10.1016/j.foodhyd.2022.107776

Kumar, P., Hajdu, C., Toth, A., & Horvath, D. (2021, Mar 3). Flow-driven surface instabilities of tubular chitosan hydrogel. *Chemphyschem, 22*(5), 488-492. https://doi.org/10.1002/cphc.202000952

Lacroix, I. M. E., Chen, X. M., Kitts, D. D., & Li-Chan, E. C. Y. (2017, Feb 22). Investigation into the bioavailability of milk protein-derived peptides with dipeptidyl-peptidase IV inhibitory activity using Caco-2 cell monolayers. *Food Funct, 8*(2), 701-709. https://doi.org/10.1039/c6fo01411a

Laroui, H., Dalmasso, G., Nguyen, H. T., Yan, Y., Sitaraman, S. V., & Merlin, D. (2010, Mar). Drug-loaded nanoparticles targeted to the colon with polysaccharide hydrogel reduce colitis in a mouse model. *Gastroenterology, 138*(3), 843-853.e841-842. https://doi.org/10.1053/j.gastro.2009.11.003

Le Gouic, A. V., Harnedy, P. A., & FitzGerald, R. J. (2019). Bioactive peptides from fish protein by-products. In *Bioactive Molecules in Food* (pp. 355-388). https://doi.org/10.1007/978-3-319-78030-6_29

Liu, Q., Yang, M., Zhao, B., & Yang, F. (2020, May 26). Isolation of antioxidant peptides from yak casein hydrolysate. *RSC Adv, 10*(34), 19844-19851. https://doi.org/10.1039/d0ra02644a

Lorenzo, J. M., Munekata, P. E. S., Gómez, B., Barba, F. J., Mora, L., Pérez-Santaescolástica, C., & Toldrá, F. (2018). Bioactive peptides as natural antioxidants in food products – A review. *Trends in Food Science & Technology, 79*, 136-147. https://doi.org/10.1016/j.tifs.2018.07.003

Luo, Y., & Wang, Q. (2014, Mar). Recent development of chitosan-based polyelectrolyte complexes with natural polysaccharides for drug delivery. *Int J Biol Macromol, 64*, 353-367. https://doi.org/10.1016/j.ijbiomac.2013.12.017

Ma, Z., Mondor, M., Goycoolea Valencia, F., & Hernandez-Alvarez, A. J. (2023, Sep 19). Current state of insect proteins: extraction technologies, bioactive peptides and allergenicity of edible insect proteins. *Food Funct, 14*(18), 8129-8156. https://doi.org/10.1039/d3fo02865h

Maciel, V. B. V., Yoshida, C. M. P., Pereira, S., Goycoolea, F. M., & Franco, T. T. (2017, Oct 12). Electrostatic self-assembled chitosan-pectin nano- and microparticles for insulin delivery. *Molecules, 22*(10). https://doi.org/10.3390/molecules22101707

Magalhaes, G. A., Jr., Moura Neto, E., Sombra, V. G., Richter, A. R., Abreu, C. M., Feitosa, J. P., Paula, H. C., Goycoolea, F. M., & de Paula, R. C. (2016, Jul). Chitosan/Sterculia striata polysaccharides nanocomplex as a potential chloroquine drug release device. *Int J Biol Macromol, 88*, 244-253. https://doi.org/10.1016/j.ijbiomac.2016.03.070

Marcet, I., Delgado, J., Diaz, N., Rendueles, M., & Diaz, M. (2022, Jun 15). Peptides recovery from egg yolk lipovitellins by ultrafiltration and their in silico bioactivity analysis. *Food Chem, 379*, 132145. https://doi.org/10.1016/j.foodchem.2022.132145

Menchicchi, B., Fuenzalida, J. P., Bobbili, K. B., Hensel, A., Swamy, M. J., & Goycoolea, F. M. (2014, Oct 13). Structure of chitosan determines its interactions with mucin. *Biomacromolecules, 15*(10), 3550-3558. https://doi.org/10.1021/bm5007954

Milkova, V., & Goycoolea, F. M. (2020). Encapsulation of caffeine in polysaccharide oil-core nanocapsules. *Colloid and Polymer Science, 298*(8), 1035-1041. https://doi.org/10.1007/s00396-020-04653-0

Mohan, A., McClements, D. J., & Udenigwe, C. C. (2016). Encapsulation of bioactive whey peptides in soy lecithin-derived nanoliposomes: Influence of peptide molecular weight. *Food Chemistry, 213*, 143–148. https://doi.org/http://dx.doi.org/10.1016/j.foodchem.2016.06.075

Mohan, A., Rajendran, S. R. C. K., He, Q. S., Bazinet, L., & Udenigwe, C. C. (2015). Encapsulation of food protein hydrolysates and peptides: a review. *Rsc Advances, 5*(97), 79270-79278. https://doi.org/10.1039/c5ra13419f

Moreno-Fernández, S., Garcés-Rimón, M., & Miguel, M. (2020). Egg-derived peptides and hydrolysates: A new bioactive treasure for cardiometabolic diseases. *Trends in Food Science & Technology, 104*, 208-218. https://doi.org/10.1016/j.tifs.2020.08.002

Mudalige, T., Qu, H., Van Haute, D., Ansar, S. M., Paredes, A., & Ingle, T. (2019). Characterization of Nanomaterials: Tools and Challenges. In A. L. Rubio, M. m. R. Sanz, Maria José Fabra , & L. G. Gómez-Mascaraque (Eds.), *Nanomaterials for Food Applications* (pp. 313-353). Elsevier. https://doi.org/10.1016/b978-0-12-814130-4.00011-7

Nahi, O., Broad, A., Kulak, A. N., Freeman, H. M., Zhang, S., Turner, T. D., Roach, L., Darkins, R., Ford, I. J., & Meldrum, F. C. (2022, Jun 14). Positively charged additives facilitate incorporation in inorganic single crystals. *Chem Mater, 34*(11), 4910-4923. https://doi.org/10.1021/acs.chemmater.2c00097

Neves, A. C., Harnedy, P. A., O'Keeffe, M. B., & FitzGerald, R. J. (2017, Mar 1). Bioactive peptides from Atlantic salmon (Salmo salar) with angiotensin converting enzyme and dipeptidyl peptidase IV inhibitory, and antioxidant activities. *Food Chem, 218*, 396-405. https://doi.org/10.1016/j.foodchem.2016.09.053

Nirmal, N. P., Santivarangkna, C., Rajput, M. S., Benjakul, S., & Maqsood, S. (2022, Mar). Valorization of fish byproducts: Sources to end-product applications of bioactive protein hydrolysate. *Compr Rev Food Sci Food Saf, 21*(2), 1803-1842. https://doi.org/10.1111/1541-4337.12917

Nongonierma, A. B., Cadamuro, C., Le Gouic, A., Mudgil, P., Maqsood, S., & FitzGerald, R. J. (2019, May 1). Dipeptidyl peptidase IV (DPP-IV) inhibitory properties of a camel whey protein enriched hydrolysate preparation. *Food Chem, 279*, 70-79. https://doi.org/10.1016/j.foodchem.2018.11.142

Nongonierma, A. B., & FitzGerald, R. J. (2015, Nov). Bioactive properties of milk proteins in humans: A review. *Peptides, 73*, 20-34. https://doi.org/10.1016/j.peptides.2015.08.009

O'Connell, A., Goycoolea, F. M., Gulotta, A., Holmqvist, P., Schuetz, P., & Mattsson, J. (2023). The structure and dynamics of locust bean gum in aqueous solution. *Food Hydrocolloids, 138*. https://doi.org/10.1016/j.foodhyd.2022.108446

O'Neill, G. J., Egan, T., Jacquier, J. C., O'Sullivan, M., & Dolores O'Riordan, E. (2015, Aug 1). Kinetics of immobilisation and release of tryptophan, riboflavin and peptides from whey protein microbeads. *Food Chem, 180*, 150-155. https://doi.org/10.1016/j.foodchem.2015.01.131

Okeudo-Cogan, M. C., Murray, B. S., Ettelaie, R., Connell, S. D., Radford, S. J., Micklethwaite, S., & Sarkar, A. (2023). Understanding the microstructure of a functional meat analogue: Demystifying interactions between fungal hyphae and egg white protein. *Food Hydrocolloids, 140*. https://doi.org/10.1016/j.foodhyd.2023.108606

Patil, P. J., Usman, M., Zhang, C., Mehmood, A., Zhou, M., Teng, C., & Li, X. (2022, Mar). An updated review on food-derived bioactive peptides: Focus on the regulatory requirements, safety, and bioavailability. *Compr Rev Food Sci Food Saf, 21*(2), 1732-1776. https://doi.org/10.1111/1541-4337.12911

Piovesana, S., Capriotti, A. L., Cavaliere, C., La Barbera, G., Montone, C. M., Zenezini Chiozzi, R., & Lagana, A. (2018, Jun). Recent trends and analytical challenges in plant bioactive peptide separation, identification and validation. *Anal Bioanal Chem, 410*(15), 3425-3444. https://doi.org/10.1007/s00216-018-0852-x

Potaś, J., Szymańska, E., & Winnicka, K. (2020). Challenges in developing of chitosan – Based polyelectrolyte complexes as a platform for mucosal and skin drug delivery. *European Polymer Journal, 140*. https://doi.org/10.1016/j.eurpolymj.2020.110020

Pravinata, L., Akhtar, M., Bentley, P. J., Mahatnirunkul, T., & Murray, B. S. (2016). Preparation of alginate microgels in a simple one step process via the Leeds Jet Homogenizer. *Food Hydrocolloids, 61*, 77-84. https://doi.org/10.1016/j.foodhyd.2016.04.025

Pravinata, L. C., & Murray, B. S. (2019). Encapsulation of water-insoluble polyphenols and β-carotene in Ca-alginate microgel particles produced by the Leeds Jet Homogenizer. *Colloids and Surfaces A: Physicochemical and Engineering Aspects, 561*, 147-154. https://doi.org/10.1016/j.colsurfa.2018.10.041

Raval, N., Maheshwari, R., Kalyane, D., Youngren-Ortiz, S. R., Chougule, M. B., & Tekade, R. K. (2019). Importance of physicochemical characterization of nanoparticles in pharmaceutical product development. In R. K. Tekade (Ed.), *Basic Fundamentals of Drug Delivery* (pp. 369-400). Academic Press. https://doi.org/10.1016/b978-0-12-817909-3.00010-8

Rinaudo, M., Milas, M., & Le Dung, P. (1993). Characterization of chitosan. Influence of ionic strength and degree of acetylation on chain expansion. *International Journal of Biological Macromolecules, 15*(5), 281–285. https://doi.org/https://doi.org/10.1016/0141-8130(93)90027-J

Sæther, H. V., Holme, H. K., Maurstad, G., Smidsrød, O., & Stokke, B. T. (2008). Polyelectrolyte complex formation using alginate and chitosan. *Carbohydrate Polymers, 74*(4), 813-821. https://doi.org/10.1016/j.carbpol.2008.04.048

Schatz, C., Domard, A., Viton, C., Pichot, C., & Delair, T. (2004). Versatile and efficient formation of colloids of biopolymer-based polyelectrolyte complexes. *Biomacromolecules, 5*(5), 1882–1892. https://doi.org/https://doi.org/10.1021/bm049786+

Sonaje, K., Chuang, E. Y., Lin, K. J., Yen, T. C., Su, F. Y., Tseng, M. T., & Sung, H. W. (2012, May 7). Opening of epithelial tight junctions and enhancement of paracellular permeation by chitosan: microscopic, ultrastructural, and computed-tomographic observations. *Mol Pharm, 9*(5), 1271-1279. https://doi.org/10.1021/mp200572t

Sousa, P., Borges, S., & Pintado, M. (2020, Apr 30). Enzymatic hydrolysis of insect Alphitobius diaperinus towards the development of bioactive peptide hydrolysates. *Food Funct, 11*(4), 3539-3548. https://doi.org/10.1039/d0fo00188k

Sreekumar, S., Wattjes, J., Niehues, A., Mengoni, T., Mendes, A. C., Morris, E. R., Goycoolea, F. M., & Moerschbacher, B. M. (2022, Nov 21). Biotechnologically produced chitosans

with nonrandom acetylation patterns differ from conventional chitosans in properties and activities. *Nat Commun, 13*(1), 7125. https://doi.org/10.1038/s41467-022-34483-3

Stephansen, K., Chronakis, I. S., & Jessen, F. (2014, Oct). Bioactive electrospun fish sarcoplasmic proteins as a drug delivery system. *Colloids and Surfaces B-Biointerfaces, 122*, 158-165. https://doi.org/10.1016/j.colsurfb.2014.06.053

Takeshita, S., Sadeghpour, A., Malfait, W. J., Konishi, A., Otake, K., & Yoda, S. (2019, May 13). Formation of Nanofibrous Structure in Biopolymer Aerogel during Supercritical CO(2) Processing: The Case of Chitosan Aerogel. *Biomacromolecules, 20*(5), 2051-2057. https://doi.org/10.1021/acs.biomac.9b00246

Trapani, A., Lopedota, A., Franco, M., Cioffi, N., Ieva, E., Garcia-Fuentes, M., & Alonso, M. J. (2010). A comparative study of chitosan and chitosan/cyclodextrin nanoparticles as potential carriers for the oral delivery of small peptides [Article]. *European Journal of Pharmaceutics and Biopharmaceutics, 75*(1), 26-32. https://doi.org/10.1016/j.ejpb.2010.01.010

Vold, I. M. N., Kristiansen, K. A., & Bjørn, E. C. (2006). A study of the chain stiffness and extension of alginates, in vitro epimerized alginates, and periodate-oxidized alginates using size-exclusion chromatography combined with light scattering and viscosity detectors. *Biomacromolecules, 7*(7), 2136–2146. https://doi.org/https://doi.org/10.1021/bm060099n

Wattjes, J., Sreekumar, S., Richter, C., Cord-Landwehr, S., Singh, R., El Gueddari, N. E., & Moerschbacher, B. M. (2020). Patterns matter part 1: Chitosan polymers with non-random patterns of acetylation. *Reactive and Functional Polymers, 151*. https://doi.org/10.1016/j.reactfunctpolym.2020.104583

Xiao, B., Xu, Z., Viennois, E., Zhang, Y., Zhang, Z., Zhang, M., Han, M. K., Kang, Y., & Merlin, D. (2017, Jul 5). Orally targeted delivery of tripeptide KPV via hyaluronic acid-functionalized nanoparticles efficiently alleviates ulcerative colitis. *Mol Ther, 25*(7), 1628-1640. https://doi.org/10.1016/j.ymthe.2016.11.020

Xing, L., Liu, R., Cao, S., Zhang, W., & Guanghong, Z. (2019). Meat protein based bioactive peptides and their potential functional activity: a review. *International Journal of Food Science & Technology, 54*(6), 1956-1966. https://doi.org/10.1111/ijfs.14132

Yan, J., Zhao, J., Yang, R., & Zhao, W. (2019). Bioactive peptides with antidiabetic properties: a review. *International Journal of Food Science & Technology, 54*(6), 1909-1919. https://doi.org/10.1111/ijfs.14090

Yilmaz, T., Maldonado, L., Turasan, H., & Kokini, J. (2019). Thermodynamic mechanism of particulation of sodium alginate and chitosan polyelectrolyte complexes as a function

of charge ratio and order of addition. *Journal of Food Engineering, 254*, 42-50. https://doi.org/10.1016/j.jfoodeng.2019.03.002

Yokoyama, K., Chiba, H., & Yoshikawa, M. (1992, Oct). Peptide inhibitors for angiotensin I-converting enzyme from thermolysin digest of dried bonito. *Biosci Biotechnol Biochem, 56*(10), 1541-1545. https://doi.org/10.1271/bbb.56.1541

Yuan, H., Luo, Z., Ban, Z., Reiter, R. J., Ma, Q., Liang, Z., Yang, M., Li, X., & Li, L. (2022, Mar 21). Bioactive peptides of plant origin: distribution, functionality, and evidence of benefits in food and health. *Food Funct, 13*(6), 3133-3158. https://doi.org/10.1039/d1fo04077d

Zamora-Sillero, J., Gharsallaoui, A., & Prentice, C. (2018, Apr). Peptides from fish by-product protein hydrolysates and its functional properties: an overview. *Mar Biotechnol (NY), 20*(2), 118-130. https://doi.org/10.1007/s10126-018-9799-3

Zhang, S., Murray, B. S., Suriyachay, N., Holmes, M., Ettelaie, R., & Sarkar, A. (2021, Jan 19). Synergistic interactions of plant protein microgels and cellulose nanocrystals at the interface and their inhibition of the gastric digestion of pickering emulsions. *Langmuir, 37*(2), 827-840. https://doi.org/10.1021/acs.langmuir.0c03148

Zhang, T., Su, M., Jiang, X. X., Xue, Y. Q., Zhang, J. X., Zeng, X. Q., Wu, Z., Guo, Y. X., & Pan, D. D. (2019, May). Transepithelial transport route and liposome encapsulation of milk-derived ACE-inhibitory peptide Arg-Leu-Ser-Phe-Asn-Pro. *Journal of Agricultural and Food Chemistry, 67*(19), 5544-5551. https://doi.org/10.1021/acs.jafc.9b00397

Zhang, Y. W., Tu, L. L., Tang, Z., Wang, Q., Zheng, G. L., & Yin, L. N. (2021, Oct). pH-sensitive chitosan-deoxycholic acid/alginate nanoparticles for oral **insulin** delivery. *Pharmaceutical Development and Technology, 26*(9), 943-952. https://doi.org/10.1080/10837450.2021.1966036

Zhou, J., Chen, M., Wu, S., Liao, X., Wang, J., Wu, Q., Zhuang, M., & Ding, Y. (2020, Aug). A review on mushroom-derived bioactive peptides: Preparation and biological activities. *Food Res Int, 134*, 109230. https://doi.org/10.1016/j.foodres.2020.109230